2008

An interactive color pre-processing method to improve tumor segmentation in digital medical images

Marisol Martinez Escobar
Iowa State University

An interactive color pre-processing method to improve tumor segmentation in digital medical images

by

Marisol Martínez Escobar

A thesis submitted to the graduate faculty

in partial fulfillment of the requirements for the degree of

MASTER OF SCIENCE

Co-majors: Mechanical Engineering; Human Computer Interaction

Program of Study Committee:
Eliot Winer, Major Professor
Jim Oliver
Matthew Frank

Iowa State University
Ames, Iowa
2008

TABLE OF CONTENTS

LIST OF FIGURES

LIST OF TABLES

ABSTRACT

In the last few decades the medical imaging field has grown considerably, and new techniques such as computerized axial tomography (CAT) and Magnetic Resonance Imaging (MRI) are able to obtain medical images in noninvasive ways. These new technologies have opened the medical field, offering opportunities to improve patient diagnosis, education and training, treatment monitoring, and surgery planning. One of these opportunities is in the tumor segmentation field.

Tumor segmentation is the process of virtually extracting the tumor from the healthy tissues of the body by computer algorithms. This is a complex process since tumors have different shapes, sizes, tissue densities, and locations. The algorithms that have been developed cannot take into account all these variations and higher accuracy is achieved with specialized methods that generally work with specific types of tissue data.

In this thesis a color pre-processing method for segmentation is presented. Most tumor segmentation methods are based on grayscale values of the medical images. The method proposed in this thesis adds color information to the original values of the image. The user selects the region of interest (ROI), usually the tumor, from the grayscale medical image and from this initial selection, the image is mapped into a colored space. Tissue densities that are part of the tumor are assigned an RGB component and any tissues outside the tumor are set to black. The user can tweak the color ranges in real time to achieve better results, in cases where the tumor pixels are non-homogenous in terms of intensity. The user then places a seed in the center of the tumor and begins segmentation. A pixel in the image is segmented as part of the tumor if it's within an initial 10% threshold. This threshold is determined if the

seed is within the average RGB values of the tumor, and within the search region. The search region is calculated by growing or shrinking the previous region using the information or previous segmented regions of the set of slices. The method automatically segments all the slices on the set from the inputs of the first slice. All through the segmentation process the user can tweak different parameters and visualize the segmentation results in real time.

The method was run on ten test cases several runs were performed for each test cases. 10 out of the 20 test runs gave false positives of 25% or less, and 10 out of the 20 test runs gave false negatives of 25% or less. Using only grayscale thresholding methods the results for the same test cases show a false positive of up to 52% on the easy cases and up to 284% on the difficult cases, and false negatives of up to 14% on the easy cases and up to 99% on the difficult cases. While the results of the grayscale and color pre-processing methods on easy cases were similar, the results of color pre-processing were much better on difficult cases, thus supporting the claim that adding color to medical images for segmentation can significantly improve accuracy of tumor segmentation.

1. INTRODUCTION

The role of digital images and digital imaging processing in various technical fields has increased considerably in the past few decades. Significant applications of digital image processing are evident in astronomy, manufacturing, and law enforcement to name a few. In astronomy, digital images of star constellations are obtained by capturing the gamma-ray band; in product manufacturing, higher-energy X-rays digital images of circuit boards can be examined for flaws; and in law enforcement, digital images of license plates can be read to monitor traffic [1].

Another field that has successfully implemented digital image processing is medicine; the increase in computational technology has expanded the role of digital images and digital image processing in medicine. Medical image data such as CT/MR images can be analyzed and visualized as two-dimensional and three-dimensional data using computers, minimizing the need of invasive surgery [1]. It is now possible to store, process, and visualize vast amounts of medical information. Medical images provide tools for diagnosis, treatment, and education of pathologies and create opportunities that can benefit health care [2].

1.1 Medical Imaging

X-rays are one of the oldest techniques used for medical imaging. X-rays have a vacuum tube with a cathode and anode. The cathode is heated causing free electrons to be released toward the anode. When the electrons strike a nucleus, energy is released in the form of X-ray radiation, this energy is used by X-ray sensitive film to produce an image [1].

Today, two popular processes to obtain medical digital images in noninvasive ways are computerized axial tomography (CAT), also called computerized tomography (CT) for short, and Magnetic Resonance Imaging (MRI). In 1972, Sir Geoffrey Hounsfield introduced the first CT machine. CT technology uses X-rays to obtain images. The first scanner took several hours to obtain the raw data and several days to reconstruct the data into an image. Currently, the latest machines are capable of collecting four images in 350 ms and constructing a 512x512 image in less than a second [3].

In 1977, Paul Lauterbur and Peter Mansfield introduced the first MRI machine. MRI technology uses the electro-magnetic energy in the radio frequency (RF) to obtain medical images. Different parts of the body will emit different variations in the RF range and using these different RF ranges the MRI image is formed [4].

MRI and CT scanners produce a series of two-dimensional (2D) slices that can be combined to form a three-dimensional (3D) representation of the data, as shown in Figure 1.

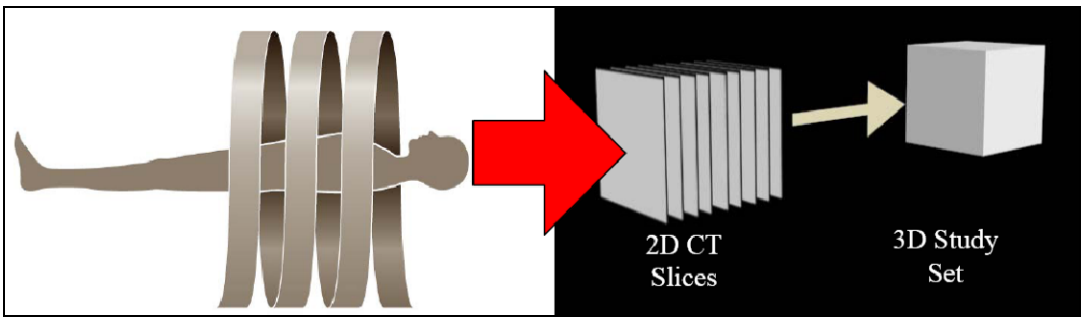

Figure 1. Representation of 2D Slices forming a 3D Set.

In the last decade medical images are being stored using the Digital Imaging and Communications in Medicine (DICOM) standard instead of the traditional 2D printed films.

The DICOM standard was developed between the American College of Radiology (ACR) and the National Electrical Manufacturers Association (NEMA) in 1993. The DICOM standard is structured as a multi-part document that facilitates the evolution of the standard since parts can be removed or added easily. These multi-parts or elements are composed of attributes, shown in Figure 2, such as a tag that works as the identifier, the length of the data, and a value field with the data [5]. This allows for a DICOM file to not only have image data but other types of data such as the patient name, age, ID, etc. Having the same format for a single file with different types of information for all patients facilitates the ease of data transfer and the implementation of software for digital processing and analysis.

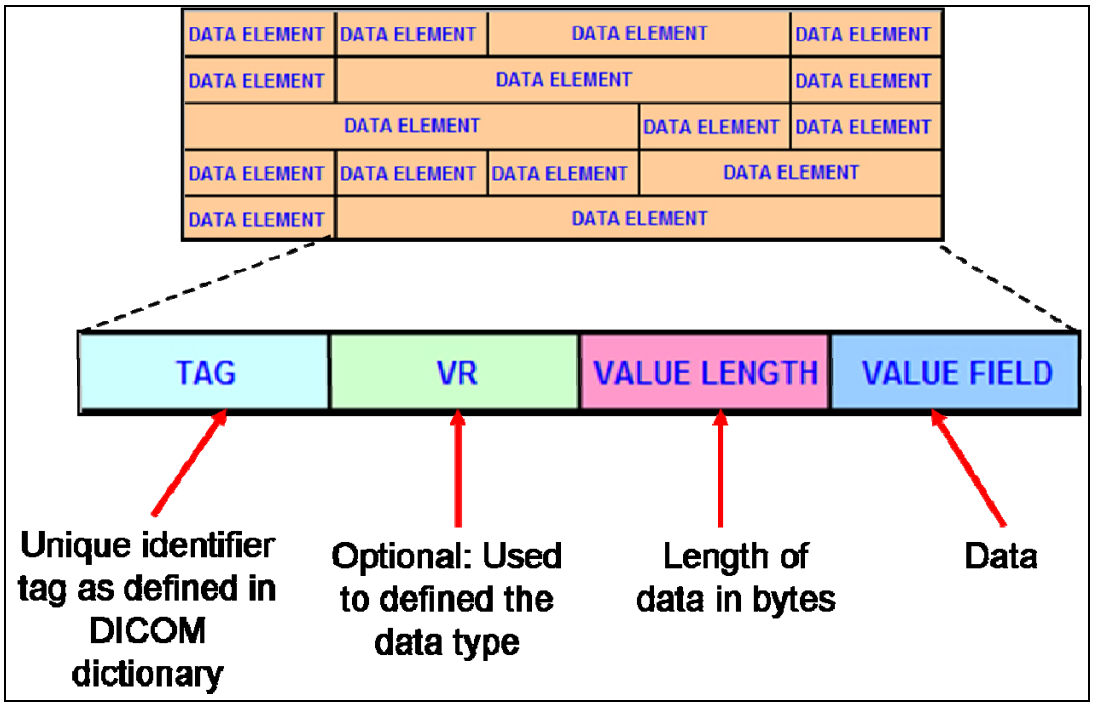

Figure 2. DICOM file structure**.**

Software packages such as Volview and OsiriX can be used to visualize these medical data by parsing the DICOM files into image and information data. The parsing process is the process of interpreting the data from the DICOM files into data usable for visualization and analysis. These packages offer different tools to manipulate the medical data and assess different information. Some of these tools include rendering a 3D volume from 2D images, clipping, and constructing animations. One of these tools is segmentation, one of the most difficult tasks in image processing.

1.2 Medical Image Segmentation

Delineation of regions of interest from an image is referred to as image segmentation. In Figure 3, the tumor on the image is circled in red; this area should be segmented from the image. Medical image segmentation plays a role in applications such as diagnosis, localization of pathologies, treatment, and education. Different segmentation algorithms have been developed for different objects of interest for example the segmentation of bone is different from the segmentation of tumor. General methods exist that can be used for different data, but higher accuracy is achieved with specialized methods. Currently there is not a single segmentation method that can be used in every medical image and still produce successful results. Figure 3 shows abdomen tumors of different patients; even from the same part of the body the tumors to be segmented have different shapes, sizes, intensity values, and locations. The algorithms try to take into account some of these variations; however they have difficulties achieving successful results. Tumors of different parts of the body add another layer of difficulty to the segmentation process, and current methods are not able to

account for all these differences [6]. Different segmentation approaches will be discussed in Chapter 2.

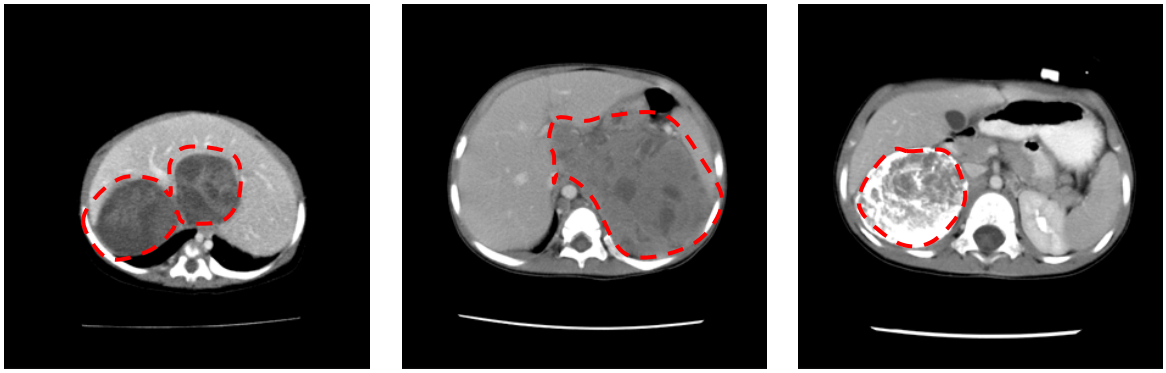

(a) Homogenous tumor (b) Fuzzy edges tumor (c) Heterogeneus tumor

Figure 3. Three different tumors of the abdomen: homogeneous tumor (a), tumor with fuzzy edges (b), heterogeneous tumor with calcification (c).

Most of the image segmentation methods today are based on grayscale techniques. Lately, with the advancement in computation technology, color segmentation has attracted more attention. One of the advantages of a color image is that it provides more information than a grayscale image, Figure 4 shows the same file, one in grayscale and another in color, it is easier to observe the different structures on the color image.

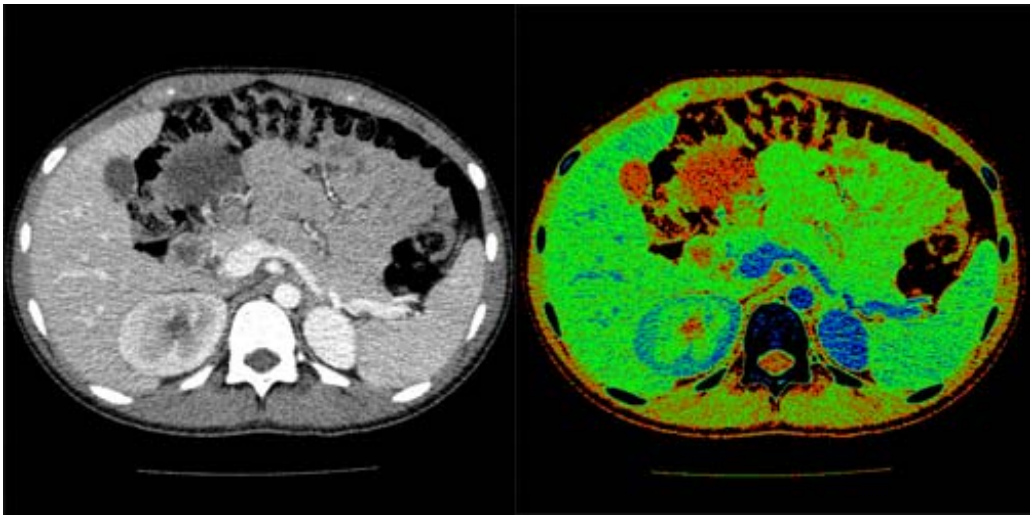

Figure 4. Grayscale and color DICOM file.

CT and MRI scans store the data in Hounsfield Units (HU) which is a measure of tissue density relative to the density of distilled water. The range of HU units in these scans is usually from -1000 HU to +1000 HU. New CT scanners can measure bigger ranges in HU. Water is assigned a HU value of zero, denser tissues such as bone have positives HU values, and less dense tissues such as fat have negative HU values [3]. Table 1 shows some HU values for different tissues [7].

Table 1. Body Tissues and corresponding HU Values.

Tissue	Value (HU)
Fat	-90
Water	0
Muscle	+44
Bone	+1005

The most common method to visualize DICOM files is to scale down the HU values into a grayscale image in a process called windowing. A window center and a window width are set according to the tissue that wants to be visualized. Any HU value smaller than the window width is set to black, and any HU value bigger than the specified window width is

set to white. The values within the width are set to the corresponding gray intensity. This process is illustrated in Figure 5.

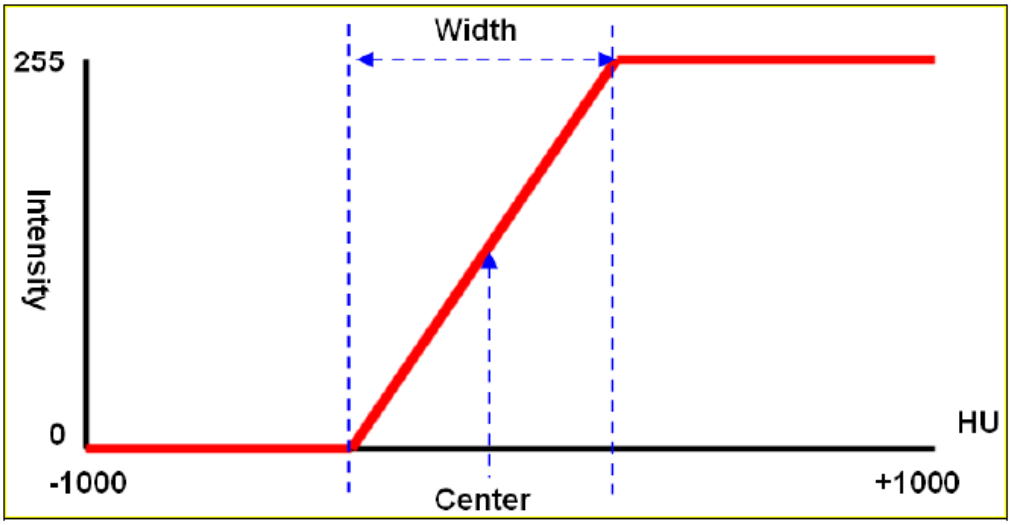

Figure 5. Windowing Process. HU values to pixel intensities.

In the windowing process the HU values are scaled down into grayscale values. Converting HU values into color is not a trivial problem to implement. A technique to map the HU values in a DICOM file to color values and use the information for tumor segmentation is presented in this thesis.

1.3 Digital Image Processing

A digital image is a two-dimensional array of numbers that represent the intensity distribution of a spatial image. These signals are sampled at finite discrete quantities. The intensity is set to a finite number of levels. Each element of the array is called a picture element or pixel [2]. A digital image is formally defined as a two-dimensional function, *f(x,y)*, where x and y are the position of the pixel, and the amplitude of *f* at any position of the

pixel is called the intensity or gray level of the image at that point. Digital imaging processing is the manipulation of digital images to produce different output images, two common digital image processes are blurring and sharpening. Blurring is used to remove noise and detail from an image; sharpening on the other hand improves the image contrast and improves the details [1]. An example of these effects is shown in Figure 6.

(d) Original Image (e) Blurred Image (f) Sharpened Image

Figure 6. Examples of image processing techniques.

In the early 1920s the first digital images were obtained in the newspaper industry by transmitting them from a submarine cable between New York and London. One of the first digital images, shown in Figure 7(a), was obtained by encoding the image, transmitting it through a cable, and then reconstructing it on a telegraph printer on the receiving location. Initially, there were many problems with the methods used to transmit pictures, the resolution obtained by transferring an image through the cable was low which produced the pixilated image shown [1].

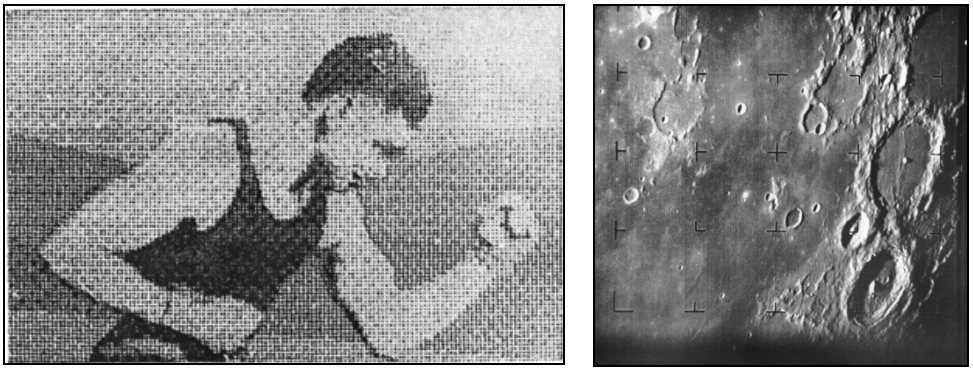

(a) Digital Image from 1920 (b) First picture of the moon

Figure 7. Examples of first digital images.

It wasn't until the 1960s when modern digital imaging processing was born. The combination between advances in computer technology and the space program allowed for the growth in the importance of digital images. The first image of the moon taken by Ranger 7 on July 31, 1964, shown in Figure 7, was processed by a computer to correct some problems with the original image [1].

The methods used to enhance the first image of the moon brought up the potential of the digital image processing field and soon these techniques were applied to other fields, especial focus was brought to medical digital images. Enhancing digital pictures were applied to medicine to improve the visualization of data for human interpretation.

1.4 Motivation

The advances in technology provide new possibilities that could potentially help in the medical field. It is now possible to look at medical data in 3D as opposed as 2D information available in the past. This has opened the medical area, offering opportunities not only to doctors but to engineers, biologists, scientists, and mathematicians. Robots that

assist in surgery such as the da Vinci surgical system [8], assisted surgery from different locations [9], and virtual reality [10] to visualize data are now a reality. Perhaps in the future robots will be able to perform surgeries automatically, and computers will be able to predict how a tumor will develop.

The tumor segmentation problem is an interesting one, it is fundamental for many other future applications in medicine and to this date there is no unique solution. Providing a set of tools for doctors to visualize tumors could beneficiate patients in many ways. In order to create these tools not only the segmentation results for the tumor extraction must be accurate but also these tools must be easy to use.

This thesis will address both areas of the problem. It will present a technique to colorize the grayscale data in DICOM files, and then use this color information to segment tumors. It will also provide software that allows the user to implement the segmentation techniques, and other visualization tools for medical data, in a fast, easy, and intuitive manner. This framework took advantage of 2D textures to allow users to manipulate segmentation data quickly, textures communicate with the graphics hardware in an efficient way to allow for fast and real time visualization of the results.

1.5 Thesis Organization

This thesis is divided into six chapters. The second chapter presents the background information with the literature review on medical segmentation, colorization of HU data, color segmentation, medical data user interfaces, and graphical hardware used with medical data. The methodology used for the segmentation algorithms and the development of the user

interface are found in chapters three and four. Chapter five presents results from the segmentation algorithms as well as the discussion of these results. And conclusions and future work are presented in chapter six.

2. LITERATURE REVIEW

2.1 Segmentation

The goal of segmentation varies from case to case. In some instances, the objective is to divide the image into groups, like gray matter, white matter, and fluids in the brain. In other cases, the purpose is to extract a single structure from the image such as a tumor in a CT scan. And some other applications have for their objective to classify the image into anatomical features such as bones, muscles, and vessels [2].

As mentioned in the introduction chapter, due to the variations in medical information there is not a general segmentation technique that can produce accurate results for every case and every goal. The literature review showed a vast and varied number of medical image segmentation methods. Most of the medical imaging segmentation techniques are based on grayscale methods [2, 11-14].

Segmentation methods discussed in this chapter can be categorized into at least one of the following groups [11]: (1) thresholding approaches (2) region growing approaches, (3) classifiers, (4) clustering approaches, (5) Markov random field (MRF) models, (6) artificial neural networks, (7) deformable models, and (8) atlas-guided approaches.

Reference [12] categorizes segmentation into two broad categories: (1) single 2D or 3D image segmentation and (2) Multi-spectral image segmentation, in which segmentation is performed on a set of images that have different grayscale values.

Taking into account the framework of this thesis, the grayscale segmentation techniques are classified into three groups: (1) classical approaches, such as thresholding and

region growing, (2) advanced approaches such as probability approaches, deformable models, fuzzy logic, and (4) hybrid approaches. These methods are covered in detail in the following sections.

2.1.1 Classical Approaches

In general, classical methods only use the information that is provided by the image [15]. Classical methods include thresholding techniques, clustering techniques and region growing techniques [2].

Thresholding techniques are characterized by using pixel intensity levels. A pixel is selected if its density is equal or less to the density set by the user [13]. If the density level of the object is significantly different from the density of the background images, then thresholding becomes a very affective and simple method for segmentation [16]. Thresholding has several limitations, classical thresholding techniques do not take into account spatial pixel relations or any other information besides grayscale density thus thresholding becomes sensitive to noise or non homogenous images, which are common occurrence in medical images [11].

Region growing is a technique in which the user places a pixel in the image, called a seed, and the region grows by adding neighboring pixels if they are within certain threshold of the current region [17]. One of the limitations of this classical technique is that it requires user input for the initial seed point. Another limitation is that selecting a pixel based on the threshold of the region makes the technique susceptible to noise. Methods that combine classical region grow with more approaches can overcome some of these limitations [18-19].

Clustering divides pixels of an image into similar groups based on their characteristics, in the case of classical methods the pixels would be grouped according to intensity values. The methods examine each pixel in an image and assign it to the group that best represents its characteristics [2, 20]. Clustering methods do not take spatial information into account either and like the rest of the classical methods they are susceptible to noise. Some algorithms have incorporated spatial information to the basic clustering techniques and have achieved better results [21].

Classical approaches are effective methods when the intensity information from the regions of interest on an image is very different from the background information. Generally, they are easy to implement and they provide fast results. However, classical methods are very susceptible to noise since they rely heavily on the intensity information of the image.

2.1.2 Advanced Approaches

Advanced approaches in segmentation include statistical approaches and probabilistic approaches, deformable models, artificial neural networks (ANNs), fuzzy logic and atlas-guided approaches.

2.1.2.1 Statistical and Probabilistic Approaches

Statistical approaches use the information on the medical image to create a statistical model of the image. These models determine if a pixel is part of the region of interest. In a similar fashion, probability approaches generate probability models that determine the probability of a pixel to be included into the segmented object [11, 15, 22 -23] Held et al., [22] developed a Markov random field model that takes the nonparametric intensity

distributions and the neighborhood correlations of the pixels to create the segmentation algorithm.

Vincken et al., [24] uses a probabilistic segmentation, in which the child pixels of the 3D image, called child voxels, are linked to more than one parent voxel. This linkage determines the final volume.

Statistical and probability methods tend to yield accurate results. However, these methods initially need to prepare models before the segmentation which causes heavy burdens on computer and time resources [15].

2.1.2.2 Deformable Models

Deformable models delineate a region of interest by using parametric curves or surfaces [11]. These curves or surfaces can move under the influence of internal forces and external forces. The internal forces, the curve or surface in itself are designed to keep the model smooth during the deformation. The external forces, computed from the image data are used to move the model toward the region of interest [25]. By combining internal and external forces deformable models tend to be robust models.

Kaus et al [26] propose a deformable model method to segment myocardium in 3D MRI. The deformable model is represented by a triangular mesh. After initially positioning the mesh, the model adapts by carrying out surface detection in each triangle of the mesh and by reconfiguration of the mesh vertices. The internal forces of this method restrict the flexibility of the segmentation by maintaining the configuration of an initial mesh. And the external forces drive the mesh towards the surface points.

One of the limitations of deformable models is that they require initial interaction from the user to set up the model and the parameters [11]. Another limitation is that deformable models are used for highly specific cases [27].

2.1.2.3 Artificial Neural Networks (ANNs)

ANNs are nodes that simulate a biological neural system. Each node has a weight associated to it that determines how the pixels should be classified [28]. Huang et al [29] developed a model that uses Neural Networks to contour breast tumors. In their method a hidden learning algorithm assigns weights to the neurons based on texture features of the image. An input vector is compared with all weight vectors and it is matched with the best neuron which corresponds to an associated output. The neural network was used as a filter for subsequent segmentation algorithms.

One of the advantages of learning algorithms is that they can be applied to a wide range of problems. One of the limitations of learning algorithms is that they have to be trained, if the training set is not large enough errors occur, the same happens if it is over trained. Another limitation is that ANN is a black-box problem, given an input, the learning algorithm gives an output, however the details of the operations are unknown: how reliable the output is, and how was the decision reached [30].

2.1.2.4 Fuzzy Logic

Fuzzy logic is a theory that represents the vagueness of everyday life, for example when cooking concepts like add hot water, put salt to taste are not crisp instructions, they allow certain liberties. Images are by nature fuzzy and fuzzy logic methods use the vagueness

concept to perform segmentation. Fuzzy connectedness methods [31-32] are clustering methods in which every pair of pixels are assigned an affinity to each other according to different parameters such as spatial relations and intensity levels. This affinity defines the fuzzy connected project. Moonis et al [33] used fuzzy logic to segment brain tumors. To determine the affinity they used the training facility 3DVIEWNIX. Using this system they painted the tumor and edema for one patient by using a paint brush, from this one patient the affinity values were calculated and used for all the subsequent studies. For each study they first selected a general rectangular region that contained the tumor, this region was used to decrease processing as the algorithm ignored anything outside of this region. Then they planted seed points on the region of interest and their fuzzy-connectedness algorithm delineated the actual tumor.

One of the limitations of fuzzy logic approaches is that the user has to choose input parameters and the affinity relations which requires a lot more initial interaction than with other methods.

2.1.2.5 Atlas-guided approaches

Atlas-guided approaches create a model by compiling information on the anatomy of the region of interest. This model or atlas is used as the reference to segment new images. It allows for the use of both spatial and intensity information of the image [11, 34]. Lorenzo-Valdes et al [34] developed a method to segment 3D cardiac images. To construct the general atlas they manually segmented 18 to 20 cycles of the heart composed of eight to ten slices of

14 adults. Using transformation algorithms they created a subject atlas, and then using a registration method they aligned the general atlas to the subject atlas.

Atlas-guided approaches are very robust if the model and the new images are similar to the training set of images, but they are not capable of segmenting accurately images that are varied to the training set. For example if the training set is of the brain the algorithm would not be able to segment abdomen images.

Advanced methods tend to achieve better results than classical techniques, but they require more input from the user, and because they have more complex equations they take more time to implement and to process than classical approaches.

2.1.3 Hybrid Approaches

Many segmentation methods do not fall within a single segmentation group as they integrate different approaches to overcome limitations and they are classified as hybrid approaches. Gibout et al [35] combined k-means, a classical clustering approach, and deformable models to create an algorithm that takes advantage of the speed of classical approaches and the accuracy of advanced approaches.

Atkins et al [36] developed a method that uses a thresholding approach and deformable models to segment the brain in MRI. The first step in the algorithm uses histogram analysis to remove noise, the second stage produces a model to identify regions of the brain, and the third step locates the boundary of the brain.

Hybrid approaches can complement the weaknesses of the methods to achieve better segmentation results but one of their limitations is that hybrid approaches tend to be more

complex than the approaches which can translate into heavy burdens in computer and time resources

2.2 Colorization

2.2.1 Color Fundamentals

The color spectrum can be divided into six regions: violet, blue, green, yellow, orange, and red. These colors do not end abruptly but blend from one color to the next. The color of an object perceived by humans is determined by the wavelength of the light reflected from the object. If an object reflects light in all visible wavelengths, the object will be perceived as white to the observer. But if the object only reflects certain wavelengths the object will exhibit a specific color. For example, objects that reflect light between wavelengths of 500 and 570 nm are perceived as having green color. Color light spans the electromagnetic spectrum from 400 to 700 nm, shown in Figure 8 and sensors in the eye are responsible for human color vision. These sensors are sensitive to red, green, and blue light. Colors are seen as a combination of these primary colors [1].

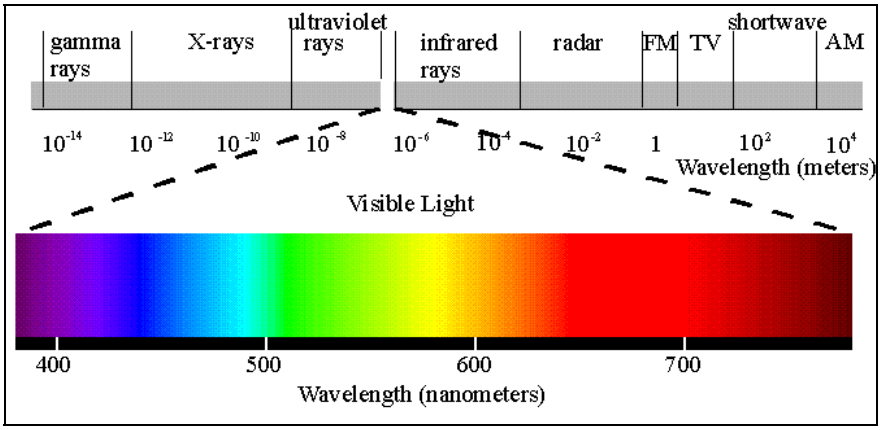

Figure 8. Electromagnetic Spectrum.

Three characteristics are generally used to describe color: brightness, hue, and saturation. Brightness is almost impossible to describe and it embodies the achromatic (without color) notion of light intensity. Hue describes the dominant wavelength in a mixture of light waves, the dominant color of an object. Saturation describes the amount of white light mixed with a hue. For example pink, the combination of red and white, is a color less saturated than red [1].

Color models or color spaces, specify the colors in a standard way by using a coordinate system and a subspace in which each color is represented by a single point [1]. The most common color spaces used in image processing methods are RGB and HIS.

The red, green, and blue (RGB) color space can be represented in a 3D cube, shown in Figure 9, color can be represented by the combination of the reg, green, and blue colors. This color space is commonly used for television systems and pictures of digital cameras [37].

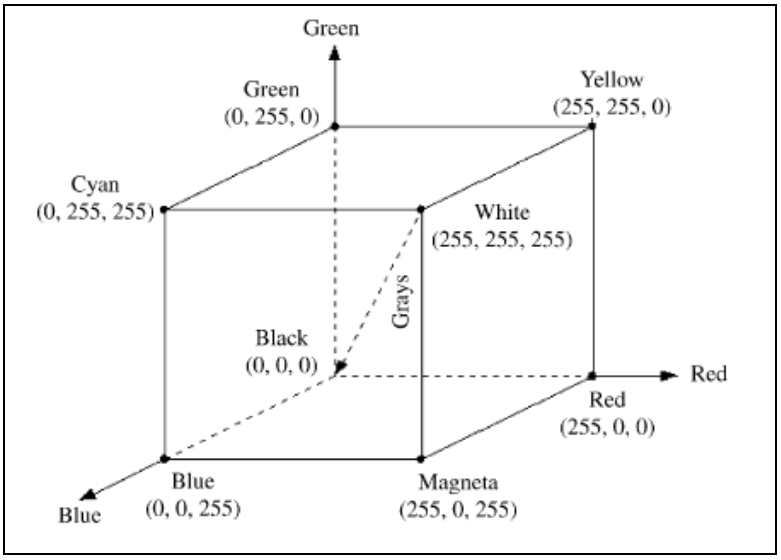

Figure 9. Representation of the RGB color space.

The Hue-Saturation-Intensity (HSI) color space separates the color information of an image from the intensity information. Hue and saturation represent color values. Hue, Saturation and Intensity were defined earlier in this section of the chapter . The HSI colors can be obtained from the RGB colors with the following formulas [37]:

$$H = \arctan\left(\frac{\sqrt{3}(G-B)}{(R-G)+(R-B)}\right) \tag{1}$$

$$I = \left(\frac{R+G+B}{3}\right) \tag{2}$$

$$S = 1-\left(\frac{\min(R,G,B)}{I}\right) \tag{3}$$

2.2.2 General Colorization Concepts

Colorization is the process of adding color to a grayscale image by the use of a computer. It is a difficult and time-consuming process, and automatic algorithms are not accurate enough and existing methods usually require extensive user input [38]. The problem of colorization is assigning three-dimensional information to a pixel from the original one-dimensional image. Colorization in RGB will add color channels to the image from 1 channel to 3 channels which will increase the possible number of colors from 256 to 16 million. With the current colorization techniques there is not a unique solution that will specify which of those new 16 million colors will best represent the image, and thus so far colorization is very dependent on user input [39-40].

Transfer functions and lookup tables are two concepts used widely in the colorization field. Transfer functions are functions that take the corresponding information of the image to obtain new color information and assign this information to the data being visualized, thus every colorization method uses a transfer function. Lookup Tables (LUT) give a color output from a grayscale input. Every lookup table is obtained from a transfer function. Some colorization techniques are focused on the final colorized image, while others are focused on creating transfer functions that can be applied to the same type data [41]. Most transfer functions are obtained through a “trial and error” method. In which the user modifies the initial parameter until a good visualization is achieved [42].

2.2.3 Colorization Techniques

Some methods ask the user to use a color palette and insert colors to the grayscale image [38, 40, 43]. For example, Levin et al [38] use a method in which the user colors a selected number of pixels in certain regions of the image and the algorithm propagates the colors in the image. The premise is that neighboring pixels that have similar intensities should have similar colors. One of the advantages of this method is that the user input is minimal and the results are accurate. However the time can be significant, at least 15 seconds per image, medical data consists of sets of hundreds of images that would take a lot of time to colorize. This method only presented images that had no noise; medical data is usually noisy so the method could have very different results.

Figure 10. Colorization technique by Welsh.

Other methods use a source image to produce the colors [44]. Welsh et al [39] colorize an image by transferring color from a color image to a destination grayscale image without the need for the user to select and apply individual colors to the target image, as shown in Figure 10. A subset of pixels of the color image is used as a sample. Then each of the pixels in the target grayscale image is matched to the color pixels by using statistics. In addition, this method can also use swatches to be used as the color source. These swatches

work the same way as the color image source, it creates a subset sample. A limitation to this method is that there needs to be a source image to provide the subset sample, and this image has to be close in content to the target image. Because of the variation in medical images it may not be possible to find two source images close enough to the destination image.

Chen et al [45] propose a method in which first the source image is segmented into objects. Each object is colorized using Welsh et al [39] method and then the objects are grouped together to form the final image. The presented method only shows images without noise.

Takahiko et al [46] developed a method that colorizes an image by adding initial color seeds to the image and the colors propagate by minimizing the color difference among 4-connected pixels. This algorithm is very fast it only takes a few seconds to colorize a 256x256 pixel image. However the final results are not accurate. In addition it requires the user to pick colors and plant seeds to the source image.

2.2.4 Medical Image Colorization Techniques

As mentioned earlier CT and MRI scans do not contain color information but rather HU values that can be windowed for visualization. In order to apply color to medical data pseudocoloring methods are used.

Pseudocoloring is a common technique for adding colors to medical images. One of the simplest techniques in pseudocoloring is to slice the image into intensity planes, and assign a color to each plane. This method applies color to the image linearly [1].

Tzeng et al [47] implements a method to create a color transfer function by having the user paint a few slices of the volume data set. The user paints the regions of interest in one color, and the background data in another color. The voxels are classified by artificial neural network segmentation approach. This method only works for 3D data.

Silverstein et al [48] developed an algorithm to colorize 3D medical data for human visualization. The purpose of their work was to realistically colorize medical images to enhance surgeon's visual perception. Initially the grayscale volume was divided into main body tissues such as fat and bone. Each structure was assigned and RGB value as realistically as possible. These initial values were adjusted by a group of surgeons. The colors between tissue types were linearly interpolated. From these values luminance was calculated and added to the data generating perceptual colorization. The user can move the luminance on the data and change the perception of the colors on the image.

Pelizzari et al [49] developed a technique to render and colorize a volume from grayscale CT and MRI scans. From a transfer function each voxel in the data is assigned a weight based on visual attributes like color by using a probabilistic classification of tissue types. Rays are cast through this weighted voxel from a viewport toward the rendered pixel that accumulates the visual attributes of the transverse voxels.

2.2.5 Limitations on Colorization Techniques

There are several limitations with the colorization techniques used today. One of the limitations is that colorization techniques require a lot of user input. Some of them ask for the user to colorize some images, or pick the correct transfer functions, or add the correct image.

Since there is no way to evaluate the output image it is difficult to know if the solution is accurate. Most of the colorization techniques are focused on creating an image that is close to reality as perceived by humans. While this can prove an effective tool for diagnostic, it may not be the only alternative if other goals for colorization want to be achieved like further computer image processing.

2.3 Color Segmentation Methods

Many of the grayscale segmentation approaches can be extended to color segmentation. Color segmentation approaches include classical techniques such as thresholding, clustering, region growing, and advanced approaches such as fuzzy logic, ANN [37, 50-52].

Some of the classical thresholding techniques separate the color information and obtain histograms separately on each piece of information [51-52]. Then through a function they combined the results. Lin et al [53] used the HSI space to segment a road from the image. They converted the RGB image into HSI space. They calculated a value for each pixel by using the saturation and the intensity. Pixels were classified according to these values.

Cheng et al [54] used a fuzzy logic approach that employ the concept of the homograph to extract homogeneous regions in a color image. In the first stage they used fuzzy logic to three color components to find threshold for each color component, then the segmentation results of the three colors were combined to form color clusters. Cheng et al achieved better results than if thresholding grayscale segmentation was performed.

Verikas et al [55] proposed a color segmentation using neural networks. An image that combined cyan, magenta, and yellow colors was created resulting in an image with nine color classes. The first stage included four steps created the segmentation. The first step was a binary decision three, then the second and third step used the neural networks to create weight vectors. And lastly a fuzzy classification was used to cluster the pixels. The second stage is a region merging approach to solve over segmentation problems. This method achieved 98% correct classification.

Cremers et al [56] implemented a hybrid segmentation approach that uses a region-based level set segmentation method and statistics that can use color information to segment the object of interest. Given a set of pixel colors at each image location, the minimization of the cost functions leads to the estimation of the boundary. This algorithm is not accurate in medical images where intensity characteristics of the region of interest and the background are similar.

2.3.1 Limitations on Current Color Segmentation Methods

Color segmentation approaches can be more reliable than gray scale segmentation approaches. However, they also have limitations similar to grayscale approaches. There is not a robust general algorithm that works for all cases. Picking a color space is difficult as each color space has advantages and disadvantages. While color images offer additional more information this can also result in more problems for segmentation algorithms, for example noise is increased [37, 51-52]. Most of the current color segmentation approaches deal with images with minimal noise, and sharp contrast between the boundaries, which is

not the case for medical images, this can introduce new problems when trying to apply the current algorithms to medical data.

2.4 Visualization

2.4.1 Current Interfaces

There are several interfaces for medical image visualization. Volview [57] and OsiriX [58] are two examples. Volview, shown in Figure 11 allows for the visualization of different medical data such as DICOM files. Tools that are included are volume rendering, cropping, coloring, segmentation, filtering, and animation. Volview works on Windows XP/Vista.

OsiriX was developed for the Mac OS as an image processing tool for medical data, is shown in Figure 11. OsiriX allows for the visualization of 2D, 3D, and even medical data combined with time information to produce videos. Like Volview, OsiriX tools include volume rendering, coloring, animation, etc.

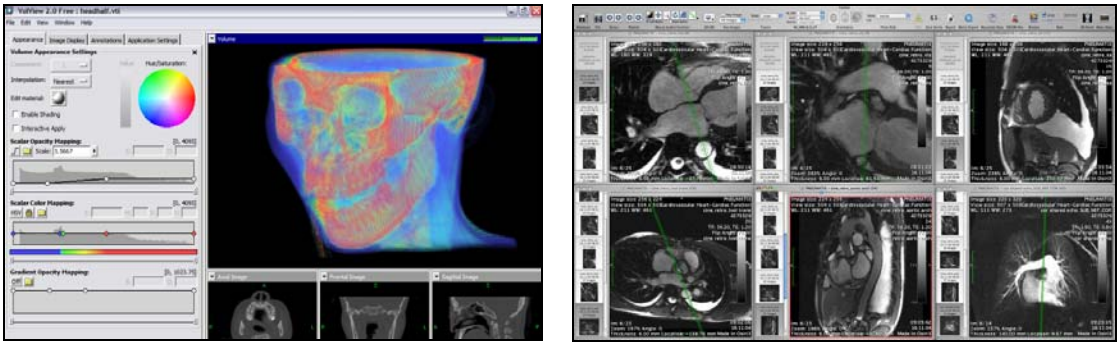

(a) Volview (b) Osirix

Figure 11. Medical Imaging Software packages.

OsiriX and Volview, as long as other medical image visualization software, allow medical staff to view and manipulate medical data in any personal computer. These tools can be used to make better assessments about the information. However there are some limitations with the current software. Osirix and Volview only work on Mac OS and Windows respectively. They are also complicated pieces of software, as shown in Figure 11, that could prove difficult to use for novice users.

2.5 Research Issues

Based on the literature review, this thesis is addressing the following research issue:

1) *To improve the accuracy and speed of tumor segmentation from medical image data using color pre-processing and interactive user inputs.*

As discussed segmentation methods currently available are still limited in a number of ways. According to the literature color segmentation improves the results over grayscale methods, however these segmentation methods have been performed when the initial input images already have the color information, which is not the case of medical data. Efforts to add color to medical data have focused on achieving good end visualization results even using segmentation algorithms to add the right colors to the corresponding tissues. Colorizing the medical data first and performing segmentation on this new information to provide better segmentation results is a new concept.

3. METHODOLOGY DEVELOPMENT

3.1 Introduction

The segmentation process takes three steps: (1) selection of region of interest and color pre-processing, (2) seed selection and segmentation, and (3) post-processing and tweaking. The first step in the process is to select the tumor to be segmented and colorize the DICOM according to the grayscale values of the tumor. During the second step the user selects a seed point in the middle of the region of interest and the algorithm segments all the slices in the data set. The process ends with post-processing that can be tweaked in real time to achieve better segmentation results. The complete segmentation process is shown in Figure 12.

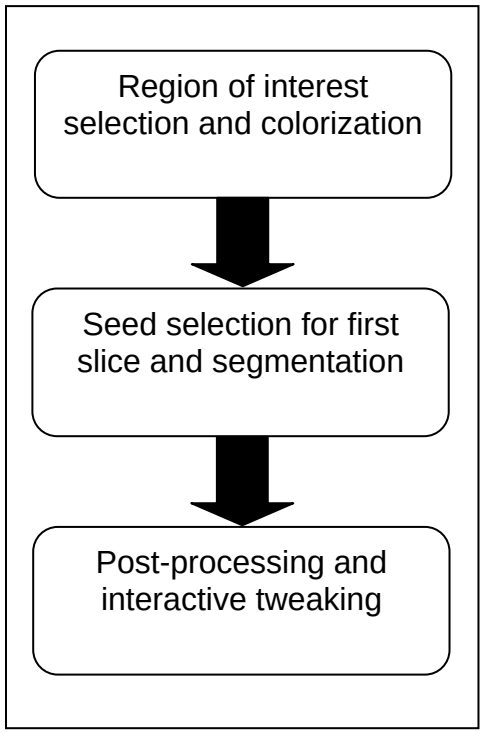

Figure 12. Diagram of the proposed Segmentation process.

3.2 Color Pre-Processing

The first step of the segmentation process is to select the region to be colorized. The original data is in HU values that usually range from -1000 to 1000. These values are usually windowed, as explained in chapter 1, to produce a grayscale image of 256 intensity levels. In this method we are adding a red, green, and blue component to the original HU values in order to provide more information that can be segmented later. The user draws the region of interest by clicking the image with the mouse. For a complex dataset, such as a highly calcified tumor with heterogeneous tissue densities, the user selection will have to be as close to the shape of the tumor as possible. In order to ensure better results the region selected has to encompass as much tumor as possible, this way more accurate input information is selected, as shown in Figure 13. In some cases where the tumor densities are very different from the healthy tissues it is not necessary to do a close selection to obtain good results. A small piece of the tumor will be sufficient, however this is only for the cases where there is a high contrast between the tumor and the healthy tissues, since a small selected region will be representative of the tumor and very different from the rest of the tissues.

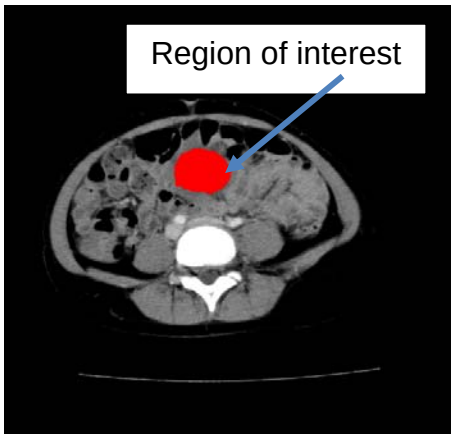

Figure 13. Selection of the region of interest that delineates the tumor.

Every point of the region selected represents a pixel with a specific HU value. From this set of values the maximum HU value and the minimum HU value are obtained and are set as the range of tissues to be colorized. Any values outside of this range are set to black since they are not considered to be a part of the tumor. The range is calculated by the difference between the HU maximum and minimum values of the region selected as shown in Equation (1):

$$HUrange = \left| HU_{\max} - HU_{\min} \right| \qquad (1)$$

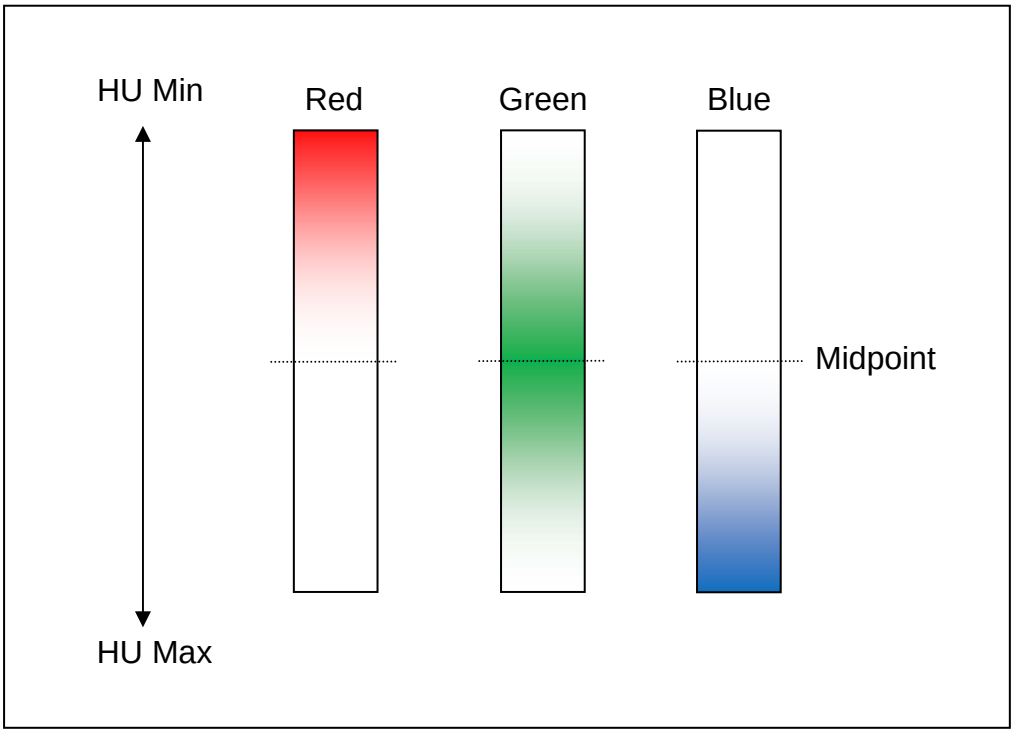

Figure 14. Colorization scheme used to assign RGB values to the pixels. The minimum HU value is set to red and the maximum HU value is set to blue.

In order to differentiate the various tissue densities, the color pre-processing scheme of Figure 14 was developed. This scheme sets the minimum value in the range to red with no

blue or green values and the maximum range is set to blue without red or green values, the rest of the values change from red to blue in a linear fashion, and any values outside the range are set to black. So any tissues that do not fall in the range to be colorized are not visible in the image and are ignored in the segmentation process to save processing time. The goal of this color pre-processing technique is not to provide color to every part of the image from a grayscale image but rather to highlight tissues of interest with color for effective segmentation.

To linearly colorize the data a parameter, P, is calculated as the ratio between the HU value of the pixel and the HU range as shown in equation (2):

$$P = \frac{HUpixelValue}{HUrange} \tag{2}$$

If this parameter is less than 0.5, then the red and green colors are calculated as shown in equations (3):

$$\begin{aligned} \mathrm{Re}\,d &= (1.0 - P \times 2) \times 255 \\ Green &= 255 \times P \times 2 \\ Blue &= 0 \end{aligned} \tag{3}$$

If P is more than or equal to 0.5 the colors are calculated as shown in euqtion 4:

$$\begin{aligned} \mathrm{Re}\,d &= 0 \\ Green &= 255 \times [1 - (P - 0.5) \times 2] \\ Blue &= 255 \times (P - 0.5) \times 2 \end{aligned} \tag{4}$$

The initial color pre-processing result of the region selection of Figure 13 is shown in Figure 15. The tumor was colorized as green and some of the tissues around it are blue. Some of the bone tissues are set to black since their HU values are outside the range of the selected region.

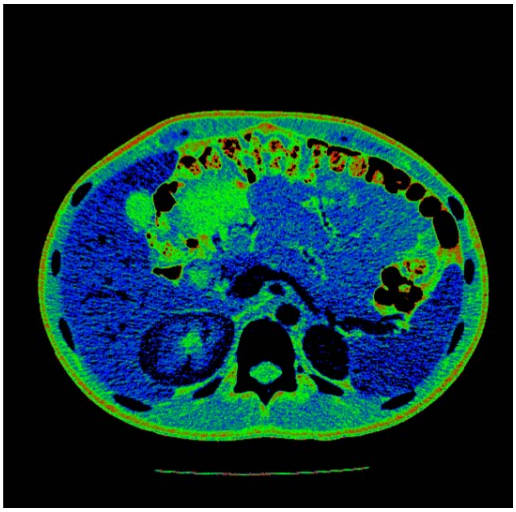

Figure 15. Sample results from the color pre-processing method.

The maximum and minimum HU values can be changed in real time to obtain different color pre-processing results, shown in Figure 16 (b) shows the color pre-processing if the small range of HU values on the DICOM file is selected. Changing the range of HU values is sometimes needed because the selected region tends to be noisy and some HU values that do not represent the tissue of interest appropriately are actually present in the selected area. The user has the option of setting the values manually if the initial color pre-processing results do not present a clear division of the different tissues.

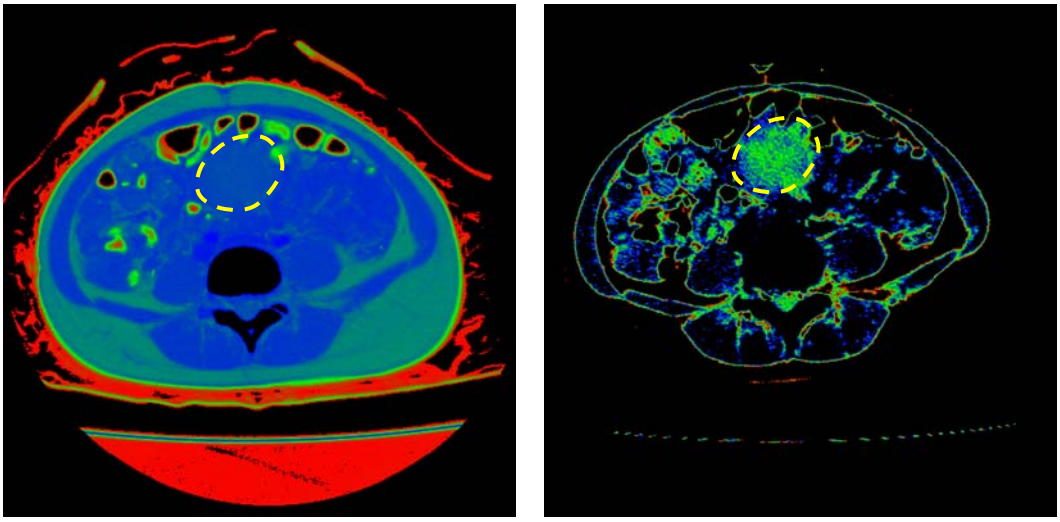

(a) HU Max: 190, HU Min: -397 (b) HU max 50 HU min -23

Figure 16. Same slice with different HU ranges show different tissues. Figure (a) shows the tumor in blue, Figure (b) shows the tumor in green and many tissues are set to black. Tumor is delineated in yellow.

Changes to the HU range are updated in real time so the user can instantly visualize the results. This is accomplished by generating OpenGL textures of the current slice. If the slice number or minimum and maximum HU values are changed, new textures are generated and displayed. For every pixel in the image the color value is calculated as described earlier in this section and the result value is set as an element of an array of 512 by 512. This array is then set as the OpenGL texture and is sent to the GPU for display. This process is analogous to making a sticker of the image, sending the sticker over and then slapping down the sticker to visualize the image, instead of sending data to the GPU pixel by pixel, which slows the color pre-processing process.

3.3 Segmentation

Since the work presented is primarily to investigate if color pre-processing can improve tumor segmentation, a simple segmentation algorithm is used instead of a more complex segmentation algorithm as a proof of concept. The segmentation algorithm selected is the basic color thresholding algorithm. Color thresholding uses RGB information instead of grayscale information. Thresholding techniques are simple methods that perform well when the tumor and the healthy tissues have high contrast in densities.

Segmentation is initialized with the user selecting a seed point within the region of interest as shown in Figure 17. From that point onwards all subsequent slices are segmented automatically.

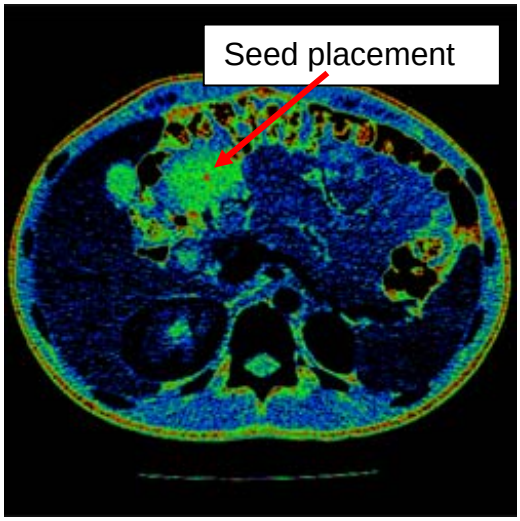

Figure 17. Example of seed placement on the colorized image.

A pixel is selected depending on two factors: distance and color. A pixel is considered a tumor pixel if it's equal or less than the threshold, initially set at 10% as shown in equation (5):

$$T_p = C \times \frac{D}{R} \tag{5}$$

T_p is the pixel threshold, C is the Color threshold, D is the distance of the pixel from the seed for that slice, and R is the search region on the slice. This search region is not a finite boundary but rather a parameter that changes the weighting when calculating the pixel threshold.

Using the region of interest, the average values of the red, green, and blue colors, A_r, A_g, A_b, are calculated. These values are then compared to the colors of each pixel, P, of the image and a color threshold, C, is obtained from the difference, the color is divided by 255 to normalize it [1] as shown in equation (6):

$$\begin{aligned} C &= \|P - A\| \\ &= \frac{\left[(P_r - A_r)^2 + (P_g - A_g)^2 + (P_b - A_b)^2\right]^{1/2}}{255} \end{aligned} \tag{6}$$

If the color maximum and color minimum are changed by the user the averages A_r, A_g, and A_b are recalculated and the final threshold is modified accordingly.

A second value, the difference between the pixel, P, and the seed, S, is calculated as shown in equation (7):

$$\begin{aligned} D &= \|P - S\| \\ &= \left[(P_x - S_x)^2 + (P_y - S_y)^2\right]^{1/2} \end{aligned} \tag{7}$$

For the first slice the seed selected by the user, as shown in Figure 17 in subsequent slices the seed moves to the center of the previous segmented region. This way the seed will move with the tumor as the tumor moves.

The search region, R, also grows or shrinks depending on how the tumor grows or shrinks as shown in equation (8):

$$R = C \times R_p \tag{8}$$

R_p is search region, of the previous slice. C_i is the percentage of growth or shrinkage and is defined as shown in equation (9):

$$C_i = \frac{3E_{i-1} + 2E_{i-2} + 1E_{i-3}}{6} \tag{9}$$

E_{i-1} is the growth rate of the tumor in the previous slice and is defined as follows (10):

$$E_{i-1} = \frac{\text{Radius of segmented region of slice i - 1}}{\text{Radius of segmented region of slice i - 2}} \tag{10}$$

where i is the number of the current slice. For example for the first slice the sum of E_{i-1}, E_{i-2}, and E_{i-3} divided by 6 give 1.1 which makes the previous search region, in the case of the first slice the search region selected by the user to grow by 10%. For slice number 4, E_3 is the segmented region of slice 3 over the segmented region of slice 2, E_2 is the segmented region of slice 2 over the segmented region of slice 1, and E_1 is 1.1. This C calculation allows for the region to grow or shrink depending on how the tumor actually changes.

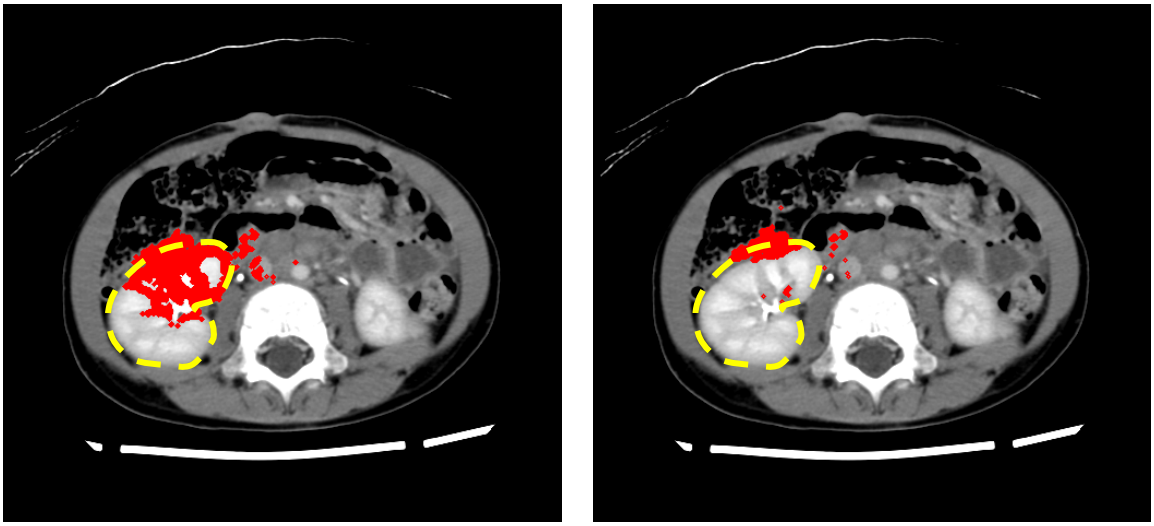

(a) Test Case #7 Max Color 222 Min Color: 24 (b) Test Case #7 Max Color 328 Min Color: -7

Figure 18. Segmentation results for test case #7 using the same threshold but different HU ranges. Figure a shows more selected pixels. Yellow line delineates the tumor.

If the final value of the pixel is lower or equal to the original threshold of 10% of the range, the pixel is selected. If the final value is higher than the threshold, then the pixel is rejected. The results of the segmentation are shown in Figure 18. The segmented object is displayed in red on top of the original DICOM file. Changing the maximum and minimum color changes the results.

Sometimes the values of the color pre-processing do not give good segmentation results. The segmentation threshold, as well as the HU maximum and HU minimum values can be tweaked in real time to give the results of Figure 18(b).

3.4 Post-Processing

Post-processing is the last step of the segmentation process. Morphological operations on the segmented pixels eliminate some of the stray pixels, or pixels that are not connected to the segmentation object. This process is performed by eroding and dilating the segmented pixels.

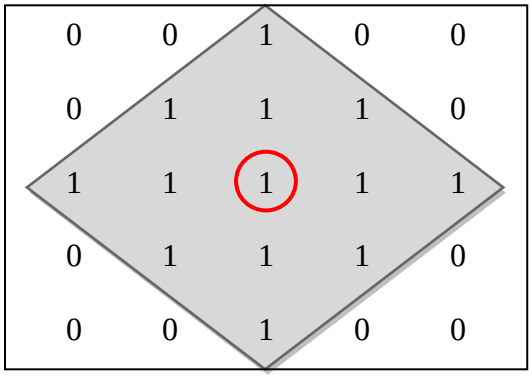

Figure 19. Example of a 5x5 structuring element.

In this case, a 5x5 diamond shaped mask, shown in Figure 19, was the structuring element selected for post-processing. Several structuring elements were tested, a 3x3, 7x7 and 9x9. After several runs it was observed that the 3x3 structuring element was too small and left too many stray pixels on the image, on the other hand the 7x7 and 9x9 structuring elements eliminated some of the tumor pixels. It was decided that the 5x5 structuring element offered the best results.

The structuring element defines the neighborhood of the pixel, which is in the center of this structuring element. In the structuring element, the zeros are pixels that should be ignored, and ones are pixels that should be included for the dilation and erosion processes,

which are highlighted in gray. This process is repeated for every pixel in the segmented region.

In erosion, the value of the pixel should be set to the minimum value of any pixels in the structuring element. Since segmentation has either a selected pixel, of value one, or a non-selected pixel, of value zero, the final value of the pixel of interest is either zero or one [59].

After erosion, dilation is performed. It follows the exact opposite process of erosion. The pixel of interest value is set to the maximum value in the structuring element, which can only be one or zero. Figure 20 shows the segmentation results with and without post-processing. Post-processing the images results in fewer stray pixels.

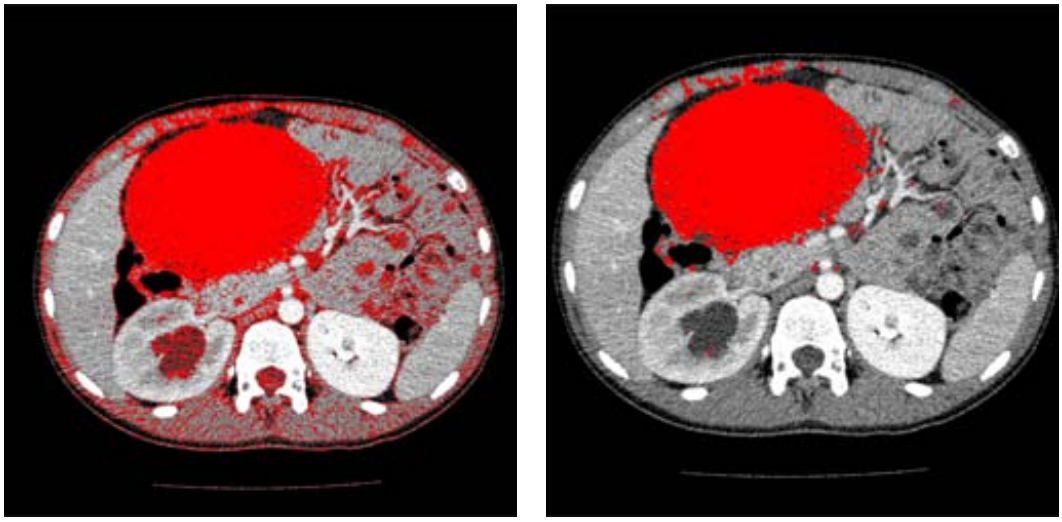

Figure 20. Segmentation without post process (left) and with post processing (right).

4. USER INTERFACE DESIGN AND DEVELOPMENT

A desktop application was developed to facilitate the visualization and analysis of medical image data and to implement the developed method. The programmatic building blocks of the software are shown in Figure 21. Using DCMTK [60], an open source library, any DICOM formatted medical image data can be processed and displayed. OpenGL[61], VTK[62], Corona[63], and VRJuggler[64] are used to manipulate the information. Corona and OpenGL draw the DICOM files in 2D, while VTK renders a volume. VRJuggler is used for communication between applications. Finally wxWidgets provides the elements to build a simple and usable graphical interface.

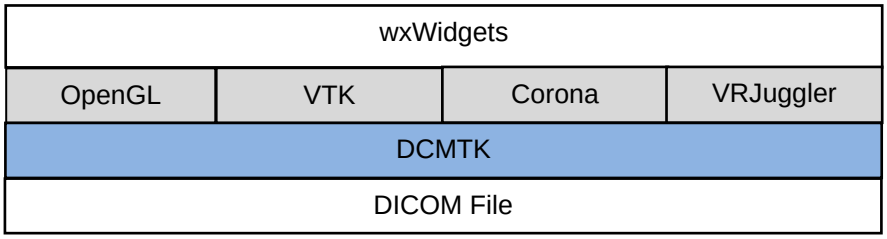

Figure 21. Programmatic building blocks for Medical Imaging Application.

4.1 Features

The software has three main features: (1) visualization, (2) segmentation, and (3) collaboration, as illustrated in Figure 22.

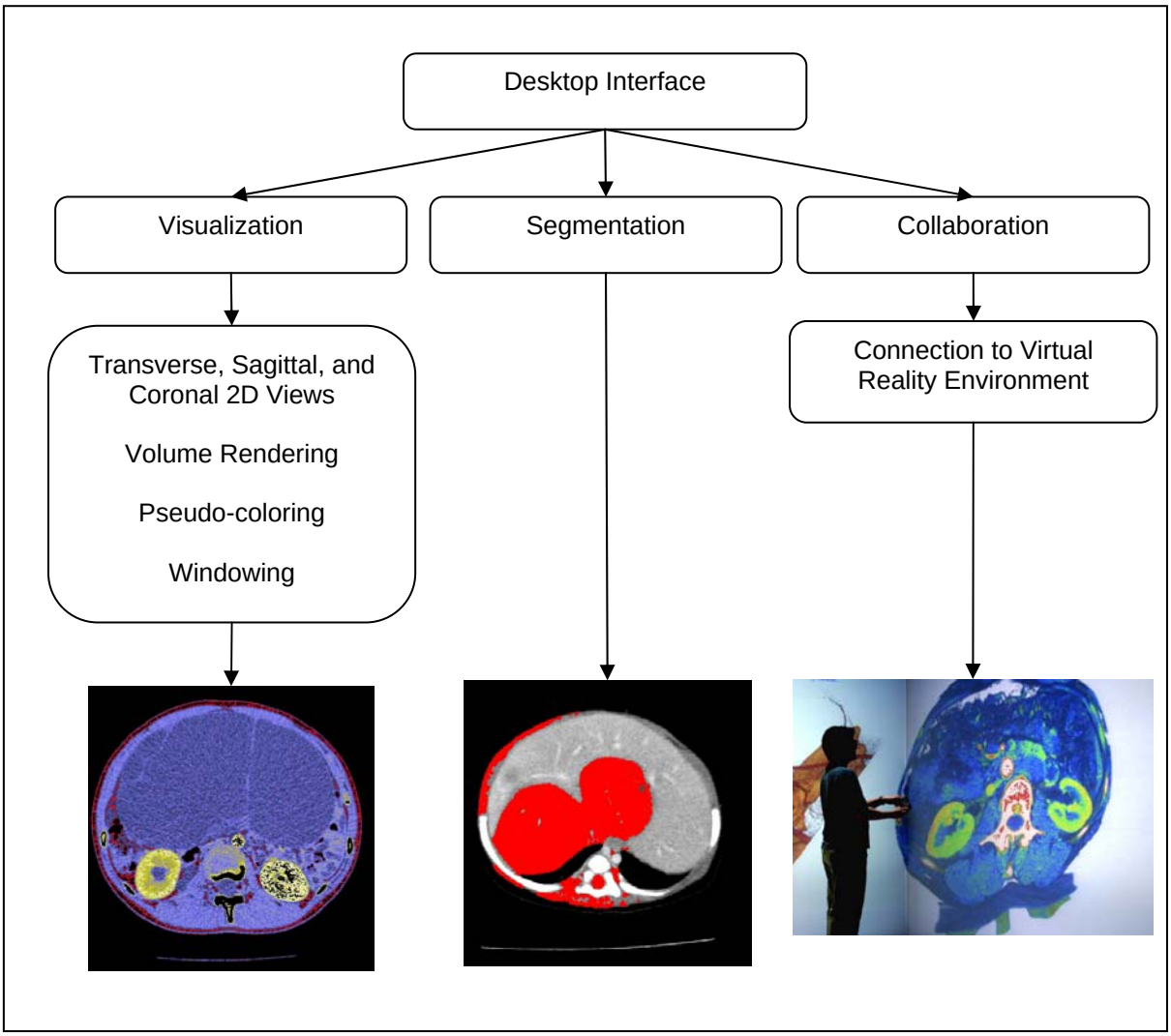

Figure 22. User interface available features: visualization, segmentation, and collaboration.

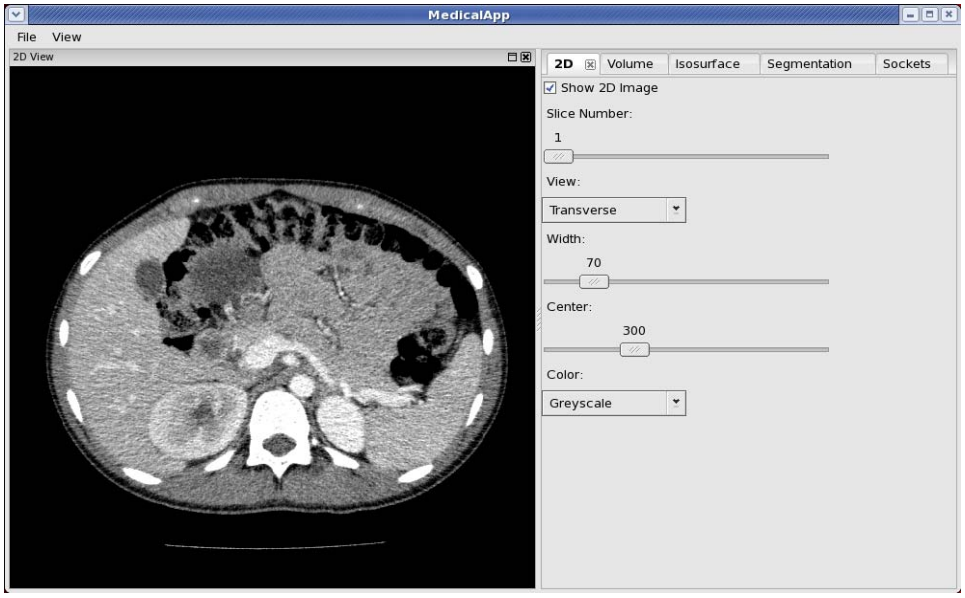

Figure 23. Application Interface highlighting the 2D tab that allows the user to see DICOM files on the left side of the frame.

A screenshot of the interface, with feature specific tabs is shown in Figure 23. There are four tabs in this application: 2D, Volume, Segmentation, and Sockets. These tabs are used to group features that are commonly used together facilitating access to the user. After opening a DICOM or a set of DICOM files the 2D tab is highlighted and the image is displayed on the left frame of the application, as shown in Figure 23.

The 2D tab allows the user to control some viewing options such as coloring, and windowing. The scrollbars allow the user to move through the slices and change the windowing set-up. The windowing process was explained in the first chapter, and an example of windowing is show in Figure 24.

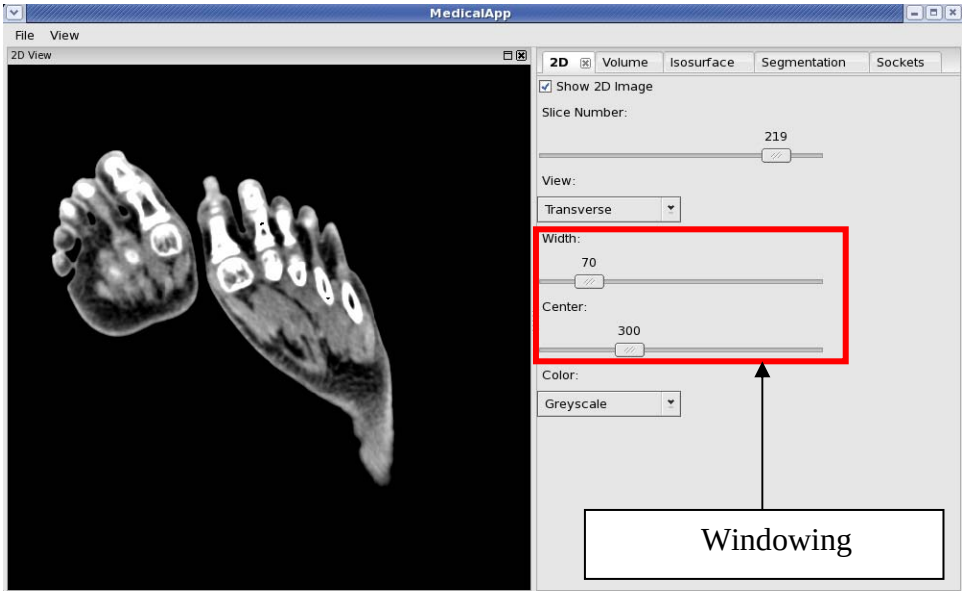

(a) DICOM not windowed Width: 70 Center: 300

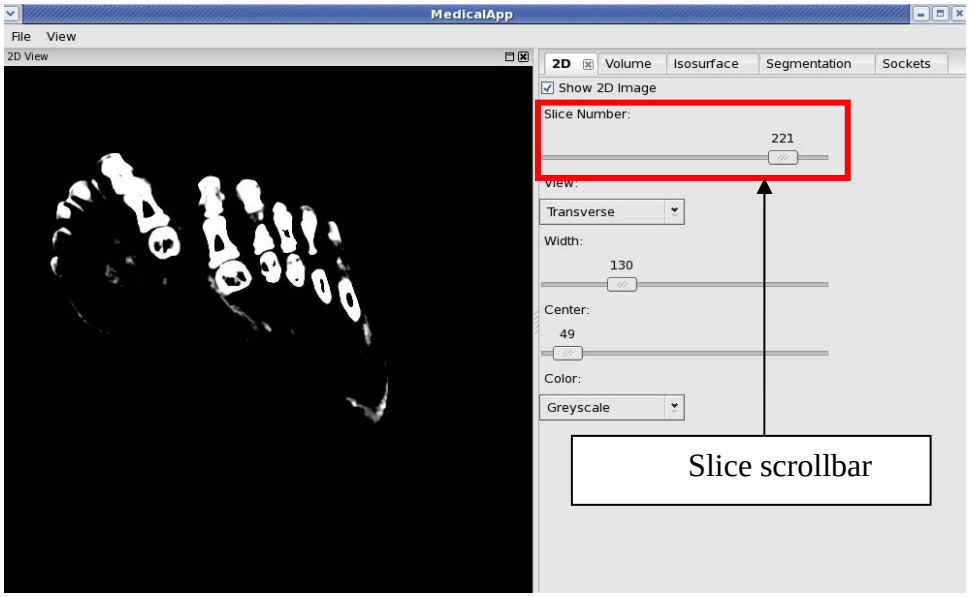

(b) DICOM windowed Width: 130 Center: 49

Figure 24. Example of a DICOM file windowed and not windowed on the Medical Interface. Windowing and slice scrollbars are highlighted in red.

Two other lists are also available, the viewing list and the pseudocoloring list. The viewing list allows the 2D slices to be seen from top-bottom (transverse), front-back(coronal), or left-right(sagittal), as shown in Figure 25.

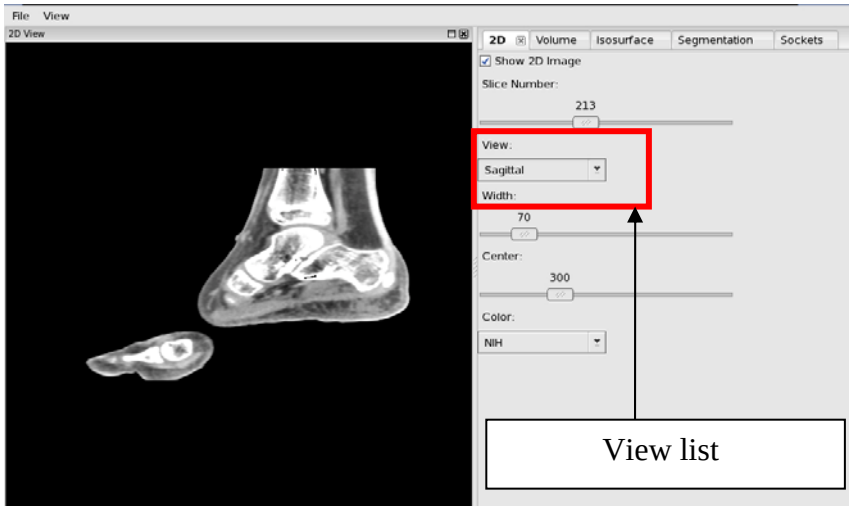

(a) Sagitall View of DICOM set

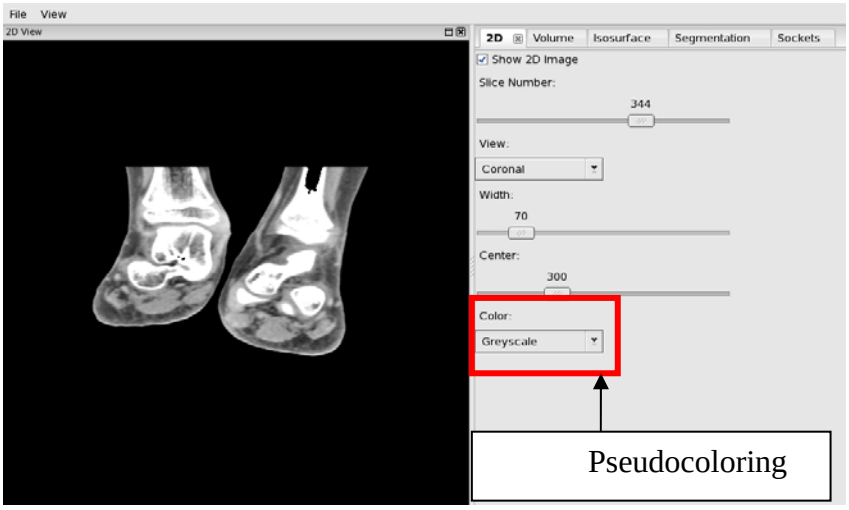

(a) Coronal View of DICOM set

Figure 25. Examples of Sagitall and Coronal View of DICOM sets. Features of 2D tab such as pseudocoloring and views are highlighted in red.

Lookup tables (LUT) are used to colorize the HU data. These LUTs are different from the ones created by the user for segmentation and were generated prior to run time. These LUTs are used for human perception and visualization. These LUTs are tables already generated that have an output color for every grayscale windowed value. They do not use the entire HU range of the DICOM file but only the 256 grayscale windowed values. This is different from the color pre-processing scheme described in the previous chapter that used the entire range of the HU values of the DICOM file. An example of pseudcoloring using the LUTs is shown in Figure 26.

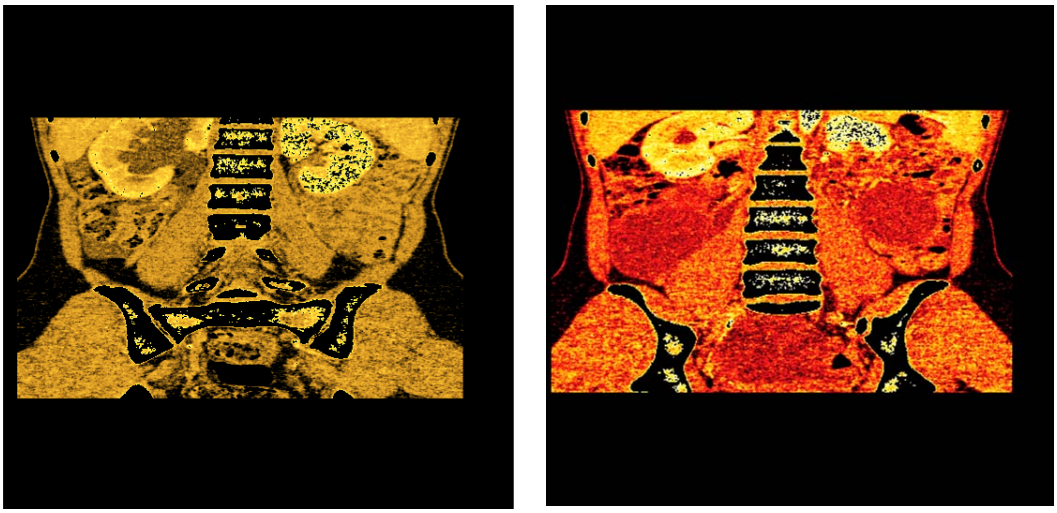

Figure 26. LUT pseudocoloring of DICOM images in the 2D tab.

Volume rendering of the image dataset is another feature of the software and is grouped together under the “Volume” tab. First, slices are sorted according to their position in the se, this position is part of the information contained in the DICOM file itself. Then the slices are stacked together to form a volume, as shown in Figure 27. VTK is used to create

the 3D volume representation of the dataset, VTK converts the pixels of the image to create a voxel, four pixels from a single slice create the front face of the voxel, and four pixels of the next slice create the back face of the voxels, VTK linearly interpolates between the front and the back face to fill the gaps and create the 3D representation of the data. The “Volume” tab of the application, shown in Figure 27, allows the user to interact with the volume through the following operations: rotate, scale, translate, and apply pseudocolor. If windowing was performed on the slices it is also represented on the volume as shown in Figure 28. Figure 29 shows different pseudocoloring for the same data set.

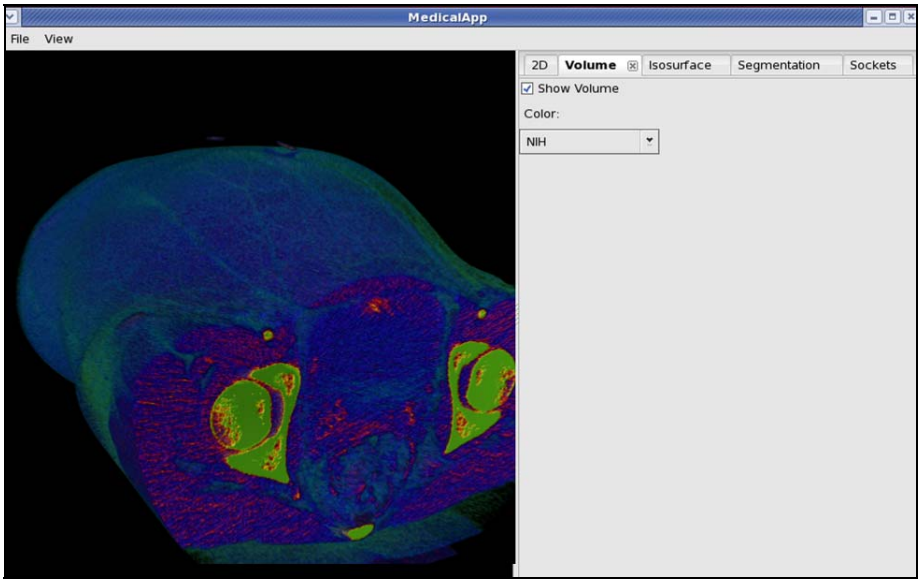

Figure 27. Example of Volume Rendering of set of DICOM files.

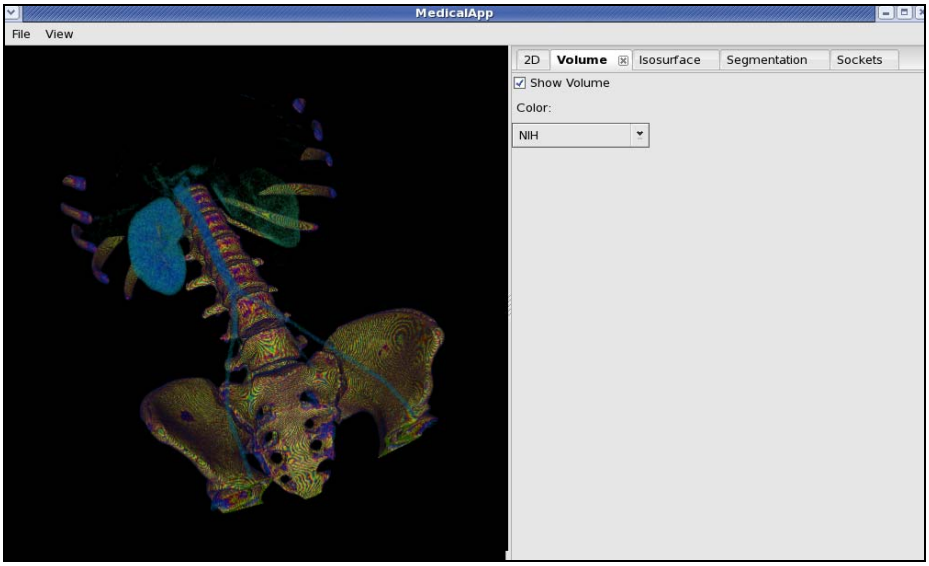

Figure 28. Windowed Volume of DICOM dataset.

Figure 29. Volume Renders with different Pseudocoloring applied.

The segmentation feature of the software was explained in the previous chapter. In this section the interface features that allow the user to perform segmentation on real time will be highlighted. The “Segmentation” tab allows the user to colorize the image and change the color range of the image on real time to highlight different tissues, as shown in Figure 30

by moving the scrollbars. After setting the ranges the user clicks on the “Do Segmentation” button and the segmentation is performed on the slice. The user can then apply the segmentation to the rest of the slices by clicking on the “Apply to All” button. The user can also change any of the scrollbars to change the segmentation results on real time as shown in Figure 30.

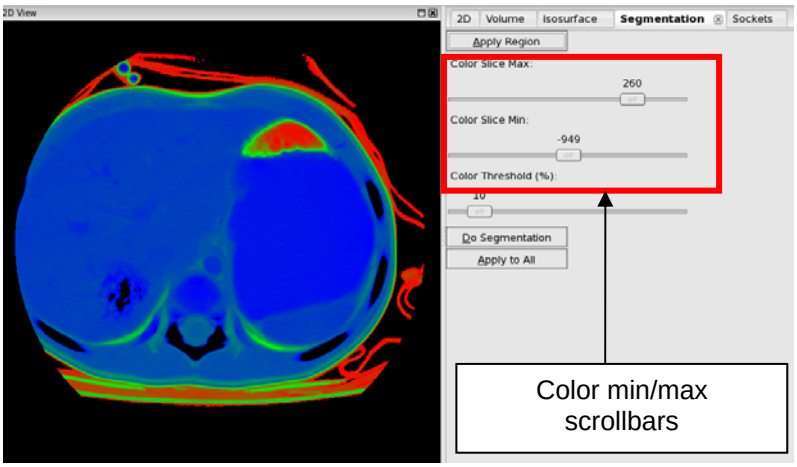

(a) Color pre-processing with Color minimum -949 Color maximum 260

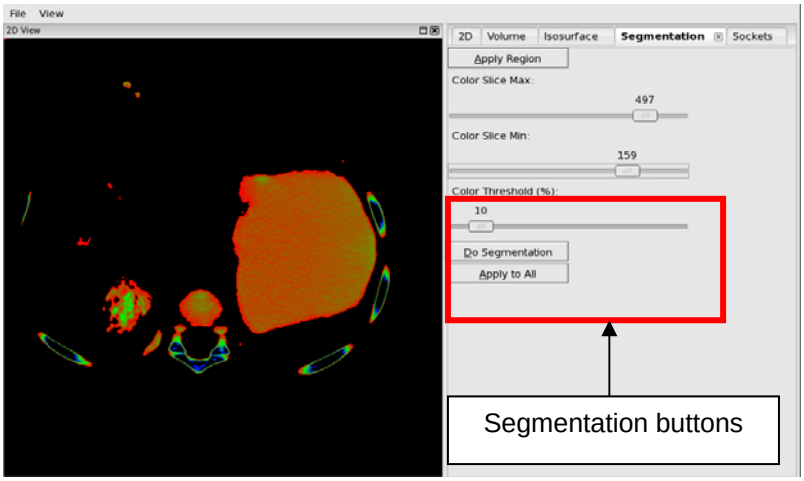

(a) Color pre-processing with Color minimum 159 Color maximum 497

Figure 30. Segmentation tab that shows different color ranges. (a) Shows most tissues because the color range is big (b) shows the tumor and some other tissues because the color range is small.

The fourth tab called “Sockets”, shown in Figure 31 was created to allow for collaboration between the virtual reality (VR) visualization software, Isis, [10] and the desktop application. Both applications can work independently but when connected any changes on the desktop will update the VR viewer in real time. These changes are sent over a network connection by using a User Datagram Protocol (UDP) socket. Every time there is a change in translation, rotation, scaling, coloring, or windowing in the desktop application a packet is sent to the VR viewer. This feature was developed to allow for two or more applications to work at the same time, so groups of people could visualize the same data to allow surgical planning.

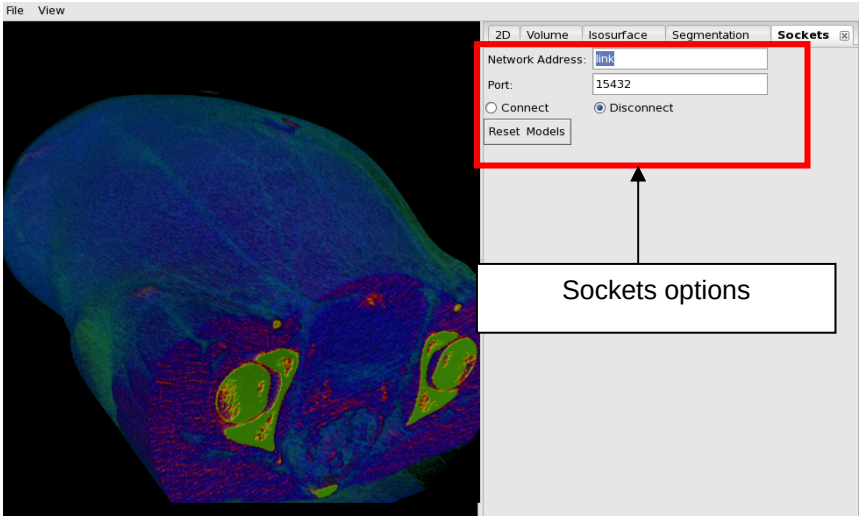

Figure 31. Example of Sockets Tab.

5. RESULTS AND DISCUSSION

5.1 Information of Test Datasets

Ten different datasets from seven individuals were used to test the developed color pre-processing and segmentation method. Test cases #1-3 were a courtesy of Dr G. Miyano from Juntendo University School of Medicine, Tokyo, Japan. Test case #1 is a Cystic Teratoma on the left ovary, #2 is an immature Teratoma, and #3 is a MucinousCystadenoma on the right ovary. Test cases #4-#10 are Neuroblastomas and the courtesy of Dr R.M. Rangayan from University of Calgary, Alberta, Canada, the different test cases are shown in Table 2 .

The test cases vary in number of slices and difficulty. There are three levels of difficulty for these data sets: tumors that have homogeneous densities are classified as a category A; tumors that have fuzzy edges and have some inhomogeneity in their tissues are considered of having a category B; tumors that have heterogeneous tissues are of category C. Some tumors with calcium buildup, which is called calcification, can be considered of category B or C depending on the degree of the calcification. When a tumor has a lot of calcification then the tissues densities in the tumors tend to be very different and the segmentation algorithms cannot easily select all types of densities in the tumor.

Table 2. Tumor Test Cases description.

Description	# Segmented Slices	Difficulty
Cystic Teratoma on left ovary	19	A
Immature Teratoma	90	A
MucinousCystadenoma on right ovary	251	A
Neuroblastoma, small and diffuse	4	B
Neuroblastoma	31	B
Neuroblastoma, some calcification	13	B
Neuroblastoma, some calcification	23	C
Neuroblastoma, highly calcified	16	C
Neuroblastoma	17	C
Neuroblastoma	12	C

5.2 Evaluation of the Segmentation Method

A common form of evaluating a segmentation algorithm is by comparing the results of a manual segmentation, performed by a trained radiologist, known as the gold standard. Radiologist Dr. J.L. Friese from Brigham and Women's Hospital, Boston, Massachusetts provided manual segmentations for test cases #1-#3, and radiologist Dr. G.S. Boag from Alberta Children's Hospital, Calgary, Canada provided manual segmentations for test cases #4-#10.

The accuracy is measured by calculating the misclassification rates of the pixels. If the segmentation algorithm classifies a pixel as part of the tumor but is not part of the golden standard that pixel is considered a False Positive (FP). If a pixel that is part of the tumor according to the golden standard is not selected by the algorithm then that pixel becomes part of the False Negative (FN). Both rates are calculated as shown in equations (10-11):

$$FP = \frac{V(A) - V(A \cap R)}{V(R)} x100\% \quad (10)$$

$$FN = \frac{V(R) - V(A \cap R)}{V(R)} x100\% \quad (11)$$

Where V(R) is the volume segmented by the radiologist, the golden standard, and V(A) is the volume segmented by the algorithm.

The FP rate indicates how the algorithm ignores healthy tissues and only segments tumor tissues. A low FP rate indicates that the algorithm correctly ignores healthy pixels. The FN rate indicates how the algorithm correctly classifies tumor pixels. A low FN rate indicates that the algorithm selects most of the tumor pixels.

The developed color preprocessing and segmentation technique was used on ten test cases. Five to six test runs were performed for each of the ten test cases and the FP and FN rates were calculated. The thresholding, HU maximum and HU minimum parameters were altered, these changes are shown in Table 3. The top two results that gave the lowest FP and FN values for each test case are discussed in detail in the following section. In addition, several of the test cases were also segmented using a grayscale thresholding method, this method was very similar to the color pre-processing method, the only difference is that instead of comparing the segmentation in the RGB channels the segmentation used only the original HU values. These additional cases provide a base line to compare how the color pre-processing, adding three channels of color to a grayscale image improve segmentation.

Table 3. FP and FN Results for all the test runs.

Dataset	Threshold	HU Max	HU min	FP	FN
1.1	0.15	124	-47	20.8245	14.8877
1.2	0.1	160	-72	22.4746	15.5382
1.3	0.2	111	-35	31.9706	11.8032
1.4	0.06	416	-230	20.1710	4.7793
1.5	0.05	416	-303	17.8671	1.9863
2.1	0.25	109	-62	12.9642	4.8015
2.2	0.1	318	-50	5.5798	10.3716
2.3	0.1	379	-87	7.997	6.7941
2.4	0.09	452	-111	11.2682	4.5689
2.5	0.07	501	-259	13.1089	3.6946
3.1	0.3	65	-100	7.2742	17.2981
3.2	0.38	65	-100	11.0837	14.0453
3.3	0.45	65	-56	10.4835	12.8215
3.4	0.17	120	-375	21.9486	10.2801
3.5	0.13	131	-121	35.9883	2.6645
4.1	0.25	109	55	54.0000	33.4583
4.2	0.25	112	41	76.8750	11.4167
4.3	0.2	112	41	50.4167	23.75
4.4	0.39	101	69	47.6250	44.0417
4.5	0.3	109	65	67.1667	37.7917
4.6	0.27	112	27	122.5	10.4583
5.1	0.08	90	-1	26.5796	54.346
5.2	0.05	574	-91	72.6124	10.821
5.3	0.11	120	-91	49.3913	22.0039
5.4	0.2	166	45	40.3981	31.7252
5.5	0.2	181	30	66.157	13.4102
6.1	0.2	590	-456	23.9025	61.7476
6.2	0.25	605	-610	40.9614	47.1893
6.3	0.4	482	98	21.9481	42.5343
6.4	0.4	574	144	14.5879	37.971
6.5	0.45	574	144	18.8161	30.1461
6.6	0.47	559	128	25.3162	26.1623
7.1	0.27	115	54	7.4111	74.2711
7.2	0.35	115	60	8.3064	72.5073
7.3	0.1	222	24	6.5087	67.8522
7.4	0.1	328	-7	5.9099	57.6397
7.5	0.08	161	-53	2.1984	87.6626
8.1	0.3	101	28	36.9001	31.7648
8.2	0.2	133	13	130.4576	11.6038
8.3	0.15	88	-62	29.2867	43.3634
8.4	0.1	178	-47	65.8532	33.7846
8.5	0.08	178	-47	50.9483	38.7746
9.1	0.2	108	-68	30.7342	40.4012
9.2	0.1	284	-85	87.5960	18.013
9.3	0.36	108	-15	42.6007	20.7052
9.4	0.28	112	-50	37.4423	22.8191
9.5	0.4	91	20	31.5722	28.5263
10.1	0.29	500	111	10.9904	48.5986
10.2	0.18	804	108	9.8529	48.2008
10.3	0.4	554	117	15.8741	38.9544
10.4	0.3	500	111	12.1784	46.9256
10.5	0.25	554	109	10.7262	49.6004
10.6	0.35	554	109	55.5239	37.0723

5.3 Hardware

The segmentation method was performed on a system with Dual AMD Opteron 250 2.4GHz processor and 4GB of memory, with a dual 512 MB NVidia Quadro FX4500 graphics cards configuration, running Linux Red Hat Enterprise edition.

5.4 Color segmentation

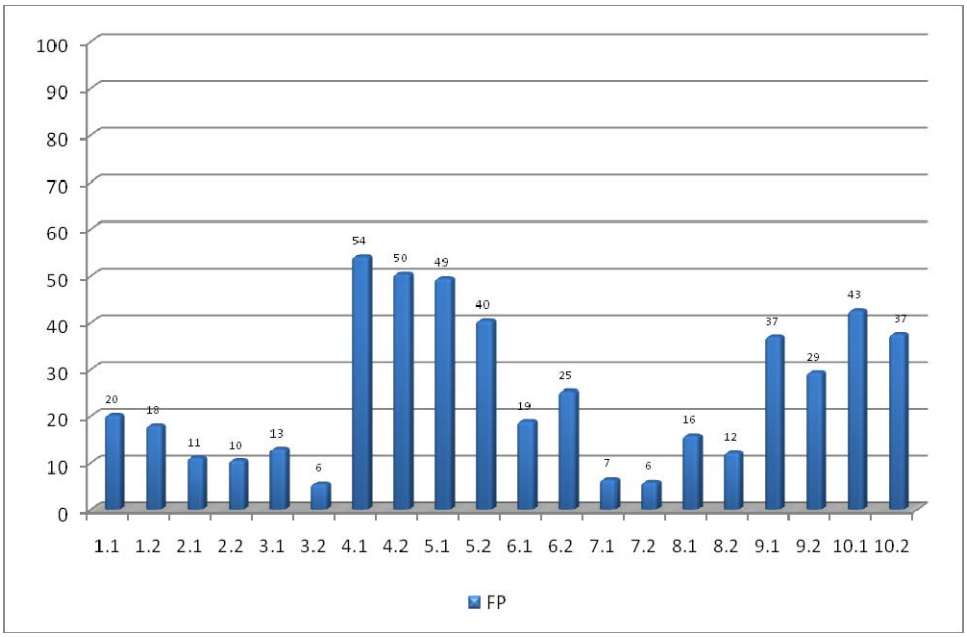

Figure 32. False positive results of the two best test runs for each test case.

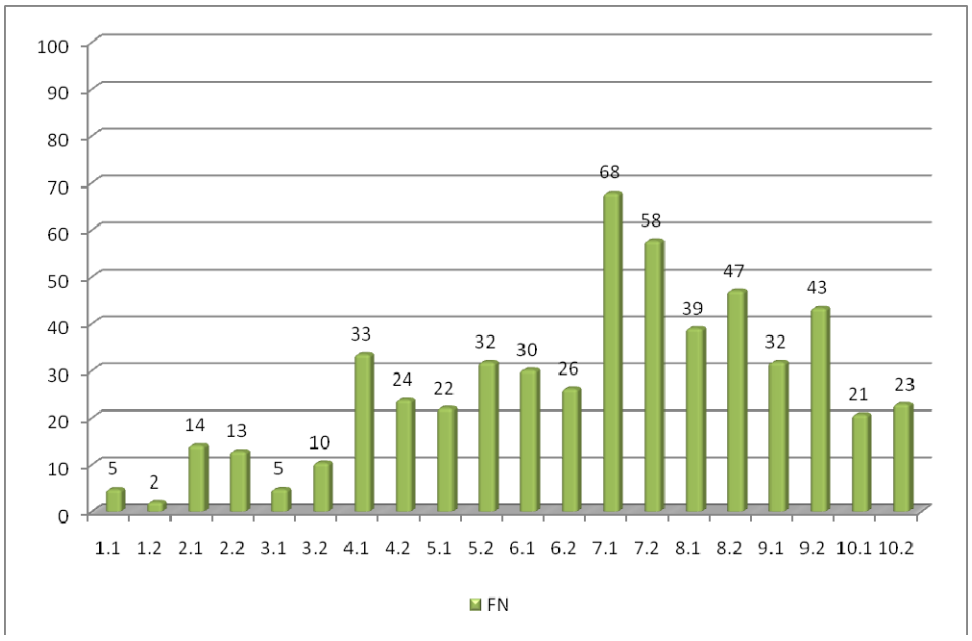

Figure 33. False negative results of the two best test runs for each test case.

Several runs for each of the test cases were conducted and the two best FP and FN rates for each test case are shown in Figure 32-Figure 33. Test Cases #1-#3 of category A have the lowest FN and FP values; Test Cases #4-#5 and Test Cases #9-#10 have the largest FP values; Test Cases #7-#8 have the largest FN values. These results are shown in detail in Table 4. These results will be discussed in detail in this section with accompanying figures.

Table 4. Results of the segmentation with color pre-processing .

Dataset	Threshold	HU Max	HU min	FP	FN
1	0.06	416	-230	20.1710	4.7793
1	0.05	416	-303	17.8671	1.9863
2	0.38	65	-100	11.0837	14.0453
2	0.45	65	-56	10.4835	12.8215
3	0.25	109	-62	12.9642	4.8015
3	0.1	318	-50	5.5798	10.3716
4	0.25	109	55	54.0000	33.4583
4	0.2	112	41	50.4167	23.75
5	0.11	120	-91	49.3913	22.0039
5	0.2	166	45	40.3981	31.7252
6	0.45	574	144	18.8161	30.1461
6	0.47	559	128	25.3162	26.1623
7	0.1	222	24	6.5087	67.8522
7	0.1	328	-7	5.9099	57.6397
8	0.4	554	117	15.8741	38.9544
8	0.3	500	111	12.1784	46.9256
9	0.3	101	28	36.9001	31.7648
9	0.15	88	-62	29.2867	43.3634
10	0.36	108	-15	42.6007	20.7052
10	0.28	112	-50	37.4423	22.8191

Test case #1 of category A yielded a FP around 20% or less and a FN of 5% or less. This showed that the color segmentation method was very successful at classifying tumor pixels as shown in Figure 34. Because the way the algorithm works, if there is a leak as shown in Figure 34(b) the region grows and more pixels are likely to be selected even if they are not part of the tumor, which lead to the FP of 20%.

Adding color information before performing segmentation is an effective way to segment the tumors when the differences between the tumor densities and the healthy densities are different.

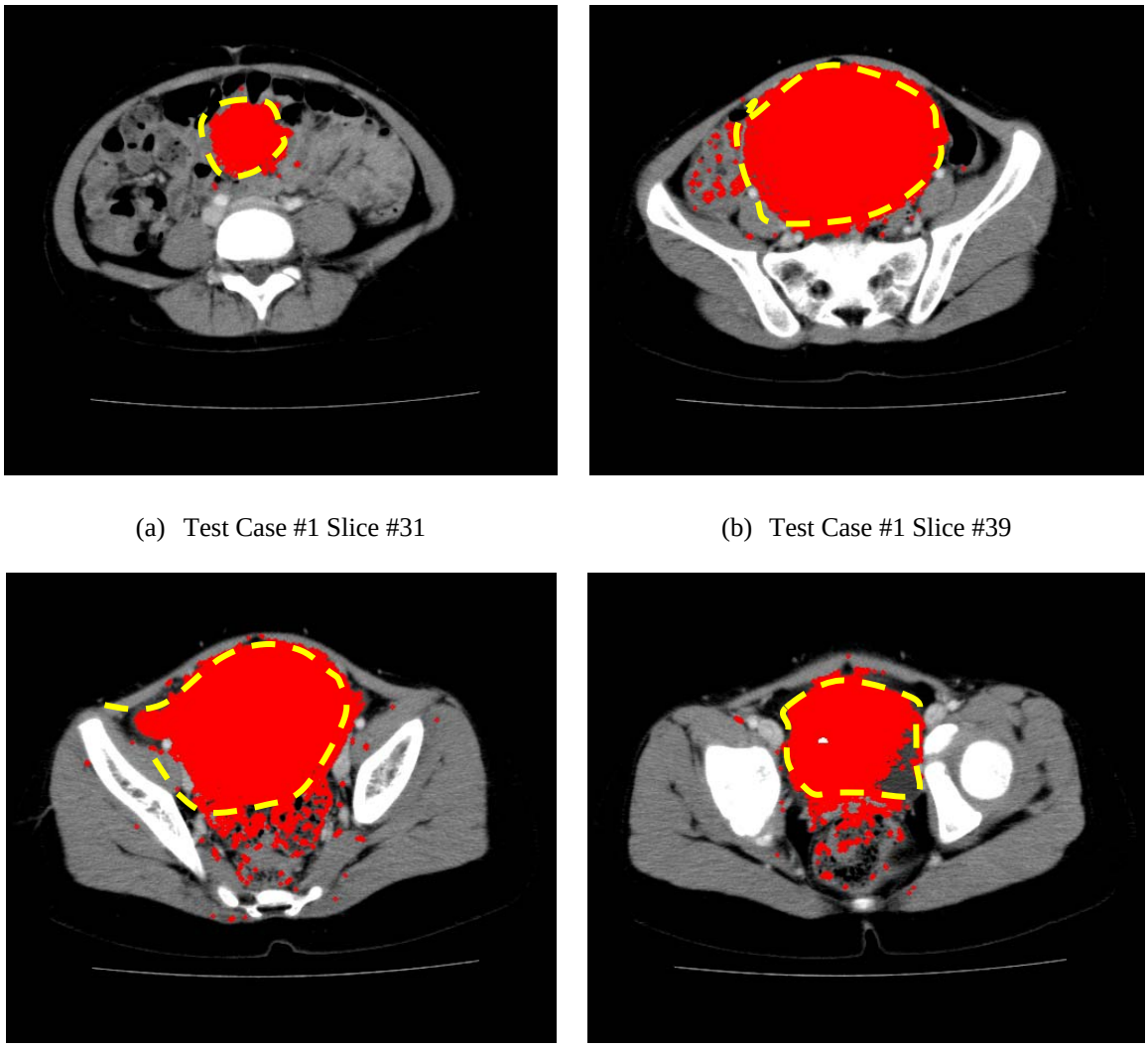

(a) Test Case #1 Slice #31

(b) Test Case #1 Slice #39

(c) Test Case #1 Slice #44

(d) Test Case #1 Slice #49

Figure 34. Test case #1 threshold 0.06. Yellow outlines tumor, red is the segmentation results by the algorithm.

Test case #2 and test case #3 had similar results as test case #1, with FP and FN values of less than 18% and as low as 5%. The reason is the same as in the previous test case, the tumor densities of these cases are very different to the densities of the healthy tissues surrounding the tumor so adding color information to the image and then thresholding these values in three channels improved the segmentation results.

(a) Region Selection

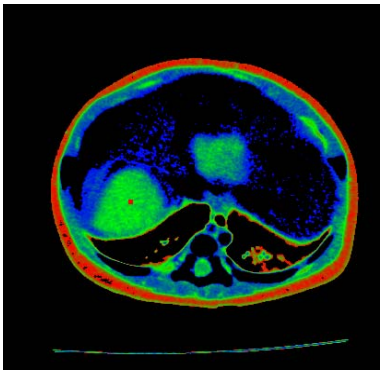

(b) Seed placement

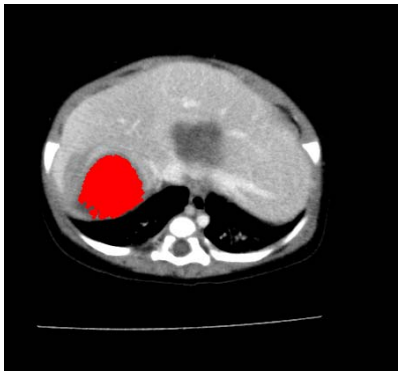

(c) Test Case #3 Slice #60

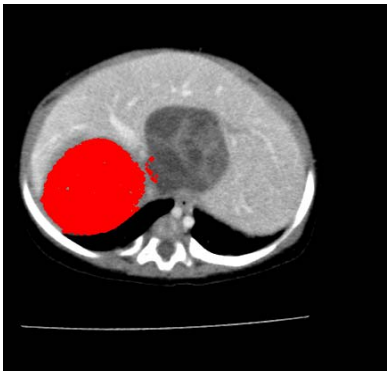

(d) Test Case #3 Slice #73

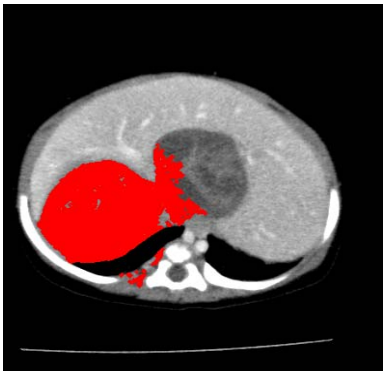

(e) Test Case #3 Slice #76

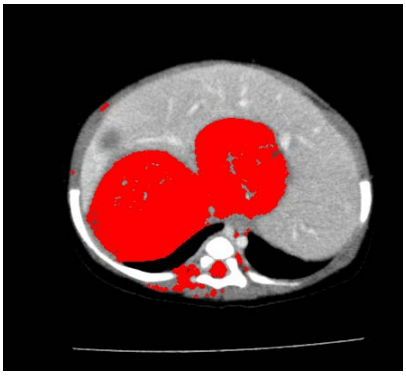

(f) Test Case #3 Slice #79

Figure 35. Test Case #3 Threshold 45%. The seed is placed on only part of the tumor and the algorithm selects both regions.

One of the strengths of this algorithm is that it can select pixels even if the tumor is divided as was the case of data set #3, as shown in Figure 35. There is only one region selected as the region of interest, shown in Figure 35(a), and only one seed placed on the region Figure 35(b). In the first slices, Figure 35(c), only one of the tumors is selected. The search region grows as the algorithm progresses, as shown in Figure 35(d), and in a few slices the algorithm segments both regions, Figure 35(e)-(f).

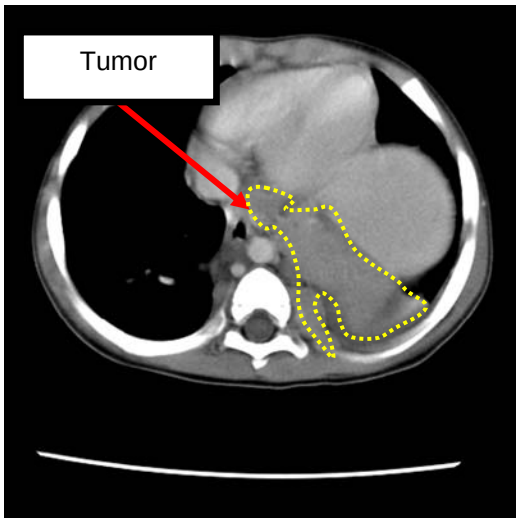

Figure 36. Test Case #5. The tumor edges have similar densities to the healthy tissues surrounding the tumors.

Test cases #4-#5, with category B, had higher FP and FN rates, with FP rates ranging from 40% to 54%. The FN rates ranged from 22% to 33%. These rates are considerably higher than the rates of the tumors from category A, because the tumor tissue densities in these cases are similar to the surrounding tissues. In addition, the edges between the tumor and the healthy tissues are similar. In some test cases the densities inside the tumor vary as shown in Figure 36. Adding color information to the image when the tumor and healthy

densities are similar, as shown in Figure 37, creates more noise and the thresholding algorithm does not perform as well. The algorithm does not classify a lot of tumor pixels that are darker than the average selected area as shown in Figure 37(b). The algorithm leaked and moved away from the tumor picking pixels that are part of the walls because they have similar densities as the original selected region.

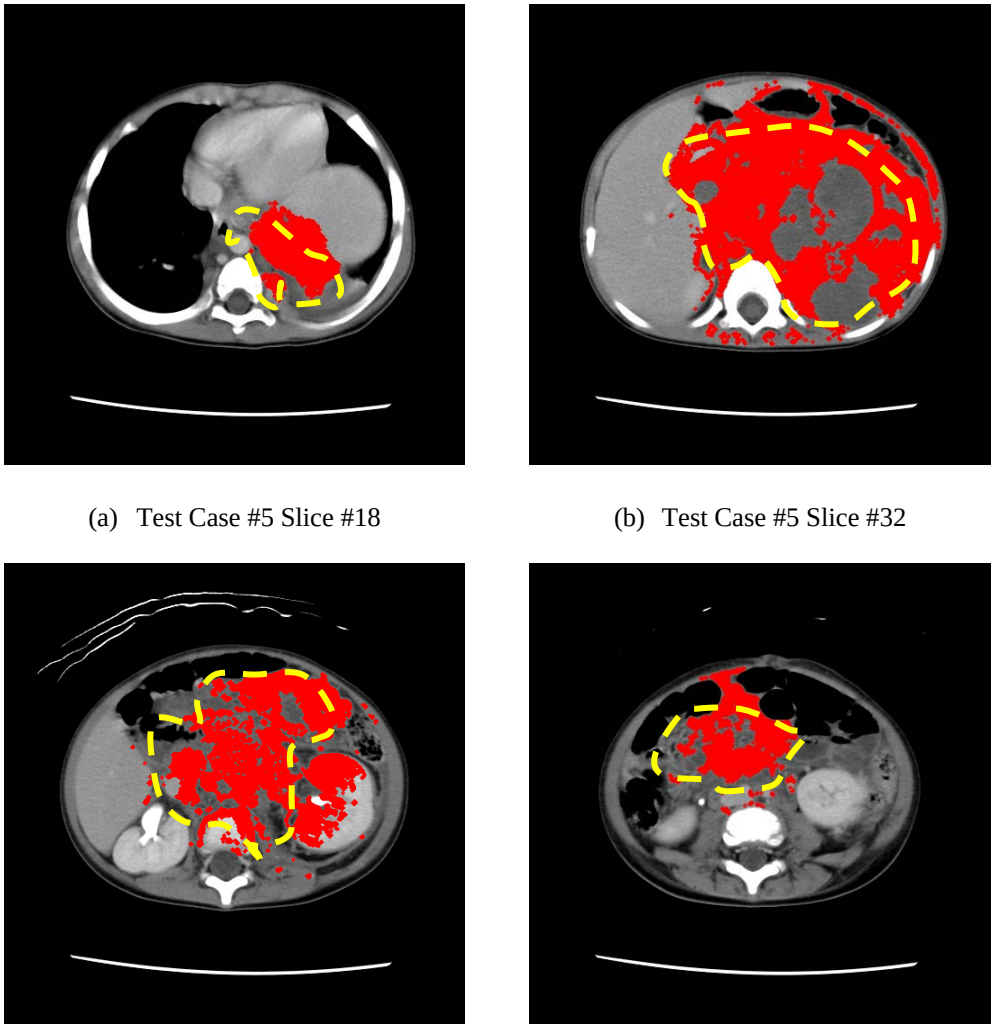

(a) Test Case #5 Slice #18

(b) Test Case #5 Slice #32

(c) Test Case #5 Slice #41

(d) Test Case #5 Slice #48

Figure 37. Test case #5 threshold 0.2. Yellow outlines the approximate tumor, red is the actual segmentation by the algorithm.

Test case #6 of category B had better FP and FN rates than the other category B cases. The best results showed a FP rate of 18% and a FN rate of 30%. This data set has calcification on the tumor, which means there is high contrast between the tumor edges and the surrounding pixels, and therefore the algorithm is capable of differentiating what is a tumor pixel and what is a healthy pixel more easily than with the other cases, as shown in Figure 38.

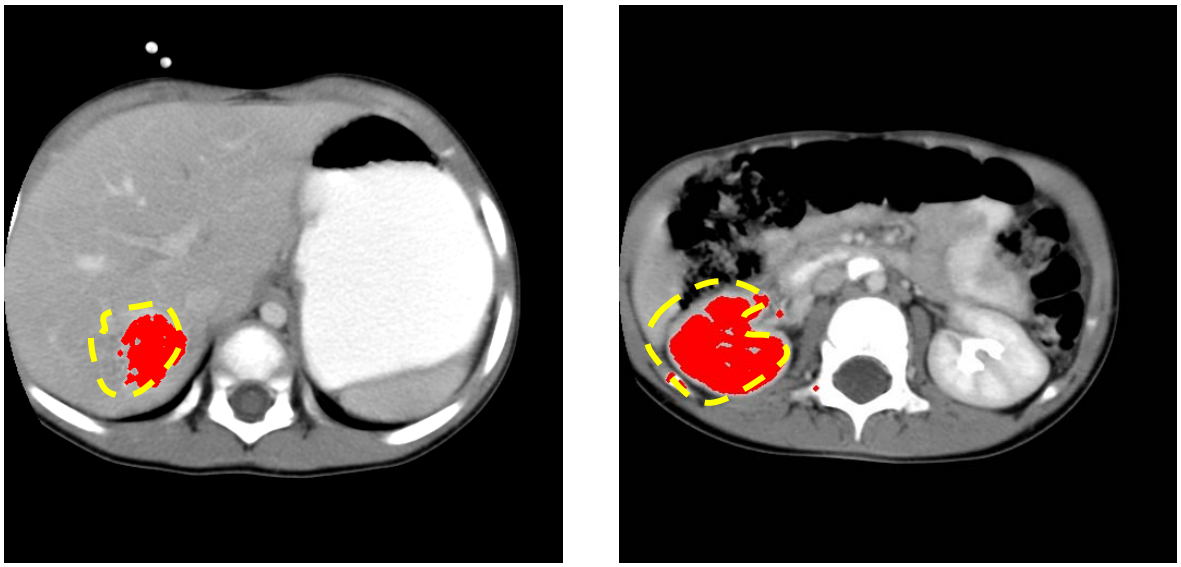

(a) Test Case #6 Slice #12 (b) Test Case #6 Slice #24

Figure 38. Test Case #6 Threshold 45%. Yellow outlines the approximate tumor, red is the actual segmentation by the algorithm.

Test cases #7 and #8 show FP values that go from 6% to 16% and FN from 38% to 67%. These two cases are similar to case #6 as the tumor in each case is calcified. Calcified tumors usually have a different density than the surrounding tissues and therefore if the right densities are used the algorithm is capable of containing the tumor. However, inside the

tumor the tissue densities may vary considerably, from calcified white colors to dark color, and therefore some of the pixels are not classified as being part of the tumor, resulting in high FN values. The results for test case #7 are shown in Figure 39.

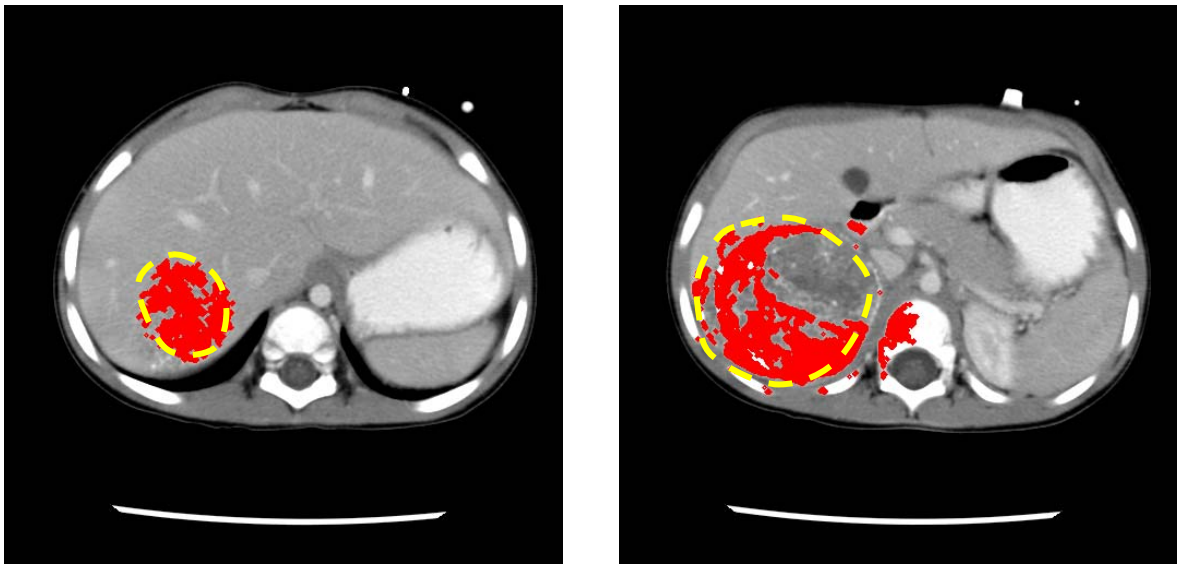

(a) Test Case #7 Slice #28 (b) Test Case #7 Slice $34

Figure 39. Test Case #7 Threshold 40%. Yellow outlines the approximate tumor, red is the actual segmentation by the algorithm.

Test cases #9 and test case #10 are not calcified, the densities of the tumor are similar to the densities surrounding the tumor. However, the tumor has a significant tissue density variation within. The results of these test cases are similar to those of test cases #4 and #5. With a FP ranging from 29% to 37% and FN from 20% to 43%. FN yielded better results, which corresponds to the fact that FP values are also high, if more pixels in general were selected then more tumor pixels were a also selected. These results are shown in Figure 40.

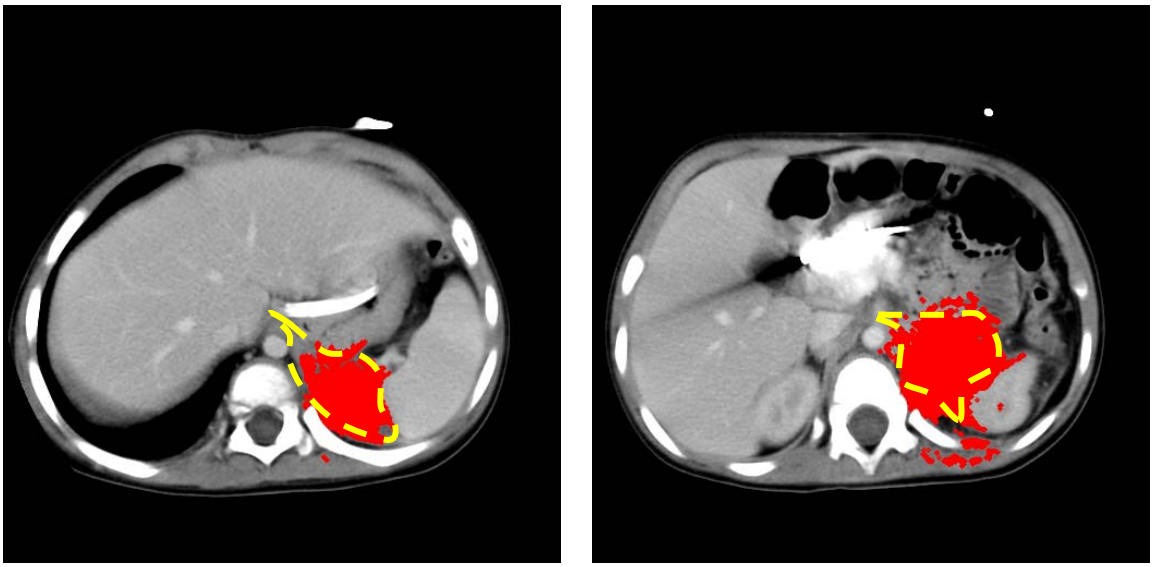

(a) Test Case #10 Slice #26 (b) Test Case #10 Slice # 33

Figure 40. Test Case #10 Threshold 28%. Yellow outlines the approximate tumor, red is the actual segmentation by the algorithm**.**

5.4.1 Summary of results

The results of the segmentation by adding color information and thresholding the colors are varied. The best results were from tumors with category A. In these cases the tumors densities and the healthy tissues densities were very different as presented in test cases #1-#3. When color is added to these cases and thresholding is done in the RGB channel the FP and FN rates are low, and most of the tumor is selected while most of the healthy tissue is not selected. Colorizing the image prior to segmentation removes unnecessary tissues such as bone and skin which allow for a simple thresholding to achieve good results.

Calcified tumors either of category B or C yielded better results than non-calcified tumors of category B and C like in test cases #6 and #7. This is due to the fact that calcified tumors also have a high contrast between the edges of the tumors and the surrounding tissues and the algorithm is successful at ignoring the healthy pixels yielding low FP, however inside

the tumors the tissue densities varied and the algorithm had problems selecting all the pixels which yielded high FN rates.

Tumors that had fuzzy edges and had high variations in their density yielded high FP and FN rates. This is because adding color information to the data and then performing a simple threshold was not enough to select tumor pixels. The colors are too close between the healthy tissues and the tumor tissues and relying heavily on tissue density differences is not enough to segment the tumor.

5.4.2 Sensitivity

This section describes the sensitivity of the segmentation results when segmentation parameters are changed. The three parameters that can be changed in the segmentation process are the thresholding, the HU maximum value and the HU minimum value. It was observed that different combinations of these parameters for the same test case would yield different results. These results are shown in Table 5.

Table 5. Standard deviation results for each of the parameters and the for each of the test runs.

	SD threshold	SD HU Max	SD HU Min	SD FP	SD FN
1	0.063008	156.7667	121.3808	5.460259	6.105034
2	0.072595	152.59	84.50266	3.295515	2.670681
3	0.135757	33.36465	127.7705	11.79481	5.508325
4	0.064395	4.262237	16.13278	28.11176	13.96728
5	0.069065	197.7756	65.48893	18.7628	17.60741
6	0.110529	43.14163	345.4597	9.041133	12.7926
7	0.12227	89.64207	46.7258	2.3456	10.88754
8	0.088204	42.02737	40.52777	40.37704	12.18777
9	0.121326	80.57171	42.22914	23.74985	8.883675
10	0.076616	113.9924	3.250641	17.92407	5.429446

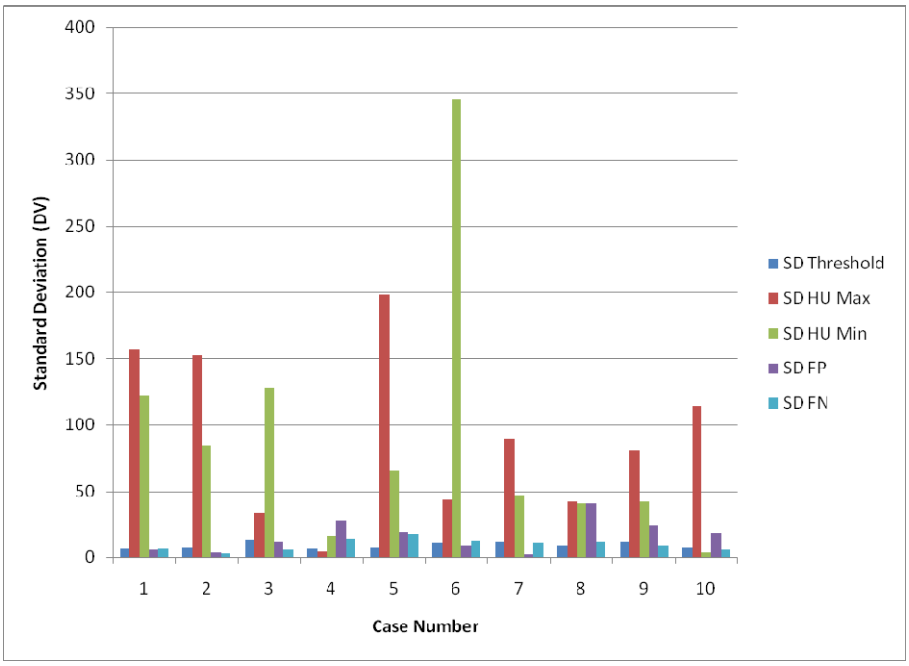

Figure 41. Standard deviation for each test case over the different test runs.

The sensitivity of the method was measured by calculating the standard deviation of each of the segmentation parameters and the standard deviation of FP and FN in the test runs, these results are shown in Figure 41 and Table 5. The range of the standard deviation for thresholding is between 0-1, for the HU values the range can be of 3000.

Test cases of category A are not very sensitive, the HU maximum and HU minimum show large standard deviations but the FP and FN standard deviations are very small they range from approximately 3% to approximately 12%. Since the HU values can show large standard deviations and yet the segmentation results show small standard deviations it seems that for test cases of Category A variations in the segmentation parameters do not affect the segmentation results.

Category B test cases show larger FP and FN standard deviations than category A. In test case #4 the standard deviation of HU maximum and HU minimum is lower, 4% and 16%

respectively than the standard deviations for FP and FN which are 28% and 14% respectively. Category B test cases are more sensitive to changes in the parameters than Category A. Category C test cases show the most erratic deviations, some test cases such as test case #7 show a FP and FN deviation of 2% and 11% than test case #8 which shows the highest standard deviation for FP of 40%. Changes in the segmentation parameters for test cases of Category B and Category C affect heavily the segmentation results because Category B and Category C tumor cases have a higher variation in tissue density within the tumor and densities between the tumor tissue and the surrounding tissues are closer, therefore these cases are very dependent on the HU values, and even small variations of HU values changes which tissues are selected and the segmentation results.

5.5 Grayscale segmentation

In this section the results of the grayscale segmentation algorithm are discussed. Several runs of test cases #1, #5, #6, and #7 were done using a grayscale thresholding segmentation algorithm. The test cases ranged from category A to category C.

To assess the effects of color pre-processing prior to segmentation, selected test cases were segmented w the original HU values using the thresholding method discussed in Chapter 3.3.

5.5.1 Algorithm

The initial region selected by the user determines the average HU value. This average was then compared to each pixel in the image and multiplied by the distance over the search

region, if the difference was the same or lower than the threshold the pixel was selected as part of the tumor.

5.5.2 Results

Table 6. Grayscale Accuracy Results.

#	Threshold	FP	FN
1	0.1	52.7817	0.6795
	0.05	21.8807	14.255
	0.08	47.8684	1.0446
5	0.06	23.6672	93.077
	0.1	71.8079	50.782
6	0.2	283.266	80.716
	0.1	224.641	99.545
7	0.1	113.4980	35.228
	0.04	19.2508	92.218

The basic thresholding method did not perform very well, the summary of the results is shown in Table 6. The rates of FP ranged from a minimum of 19% to a high of 284% the ranges of FN were from a low of 0.67% to 99%. Only in one case both the FP and FN rates were less than 22%, in the rest of the cases one of rates was at least 47%. This means that even in the case of low FP or FN rates the algorithm classified a lot of the pixels wrong either by selecting too many healthy pixels or ignoring too many tumor pixels. If the algorithm did not select tumor pixels then FP was very low while FN was large, and if the algorithm selected every pixel then FN was low but FP was large.

For Test Case #1 which is of category A the results were the best out of all the runs and test cases. The best test run on Test Case #2 presented a FP at around 21% and FN at around 14%. This is because this dataset has a high contrast between the tumor and the healthy tissues and a grayscale thresholding algorithm is able to differentiate between the tumor and the rest of the tissues, in this case the thresholding was set to 5%. However for the

same test case when the thresholding was increased to 8% the algorithm FP rate increases to around 47%. And when the threshold was set to 10% the FN decreased dramatically to .67% but FP increased to 52%, in this case FN is very small because every pixel was selected even pixels that were not part of the tumor. Even if FN rates are very low the results are not usable if many healthy pixels are selected since it will not create an accurate representation of the actual tumor.

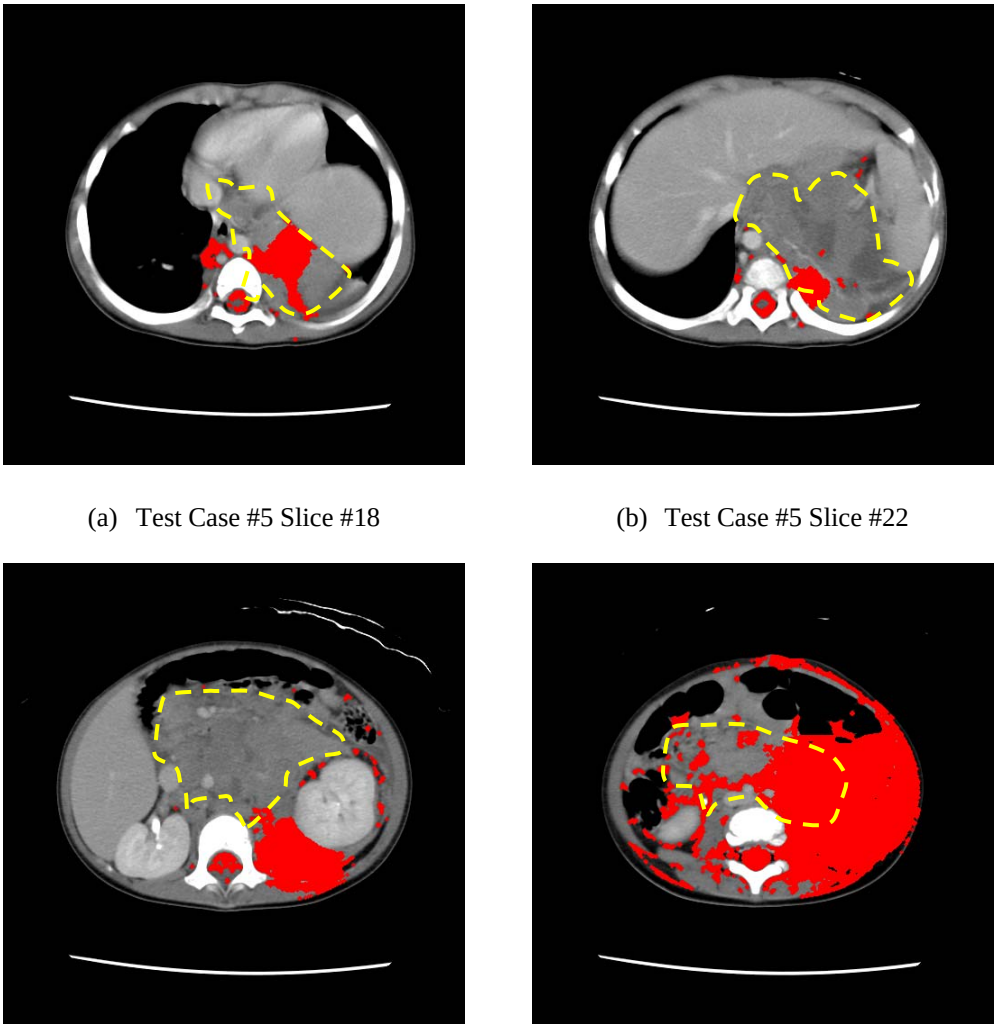

(a) Test Case #5 Slice #18

(b) Test Case #5 Slice #22

(c) Test Case #5 Slice #39

(d) Test Case #5 Slice # 48

Figure 42. Segmentation Results for Grayscale algorithm. Yellow outlines the approximate tumor, red is the actual segmentation by the algorithm.

The images of the best results for Test Case # 5 which is of category B are shown in Figure 42. The false positive is 23.67% which may seem like a reasonable result however looking at the figure it can be observed that a lot of tumor pixels were not selected which resulted in a FN of 93.077%. These results are expected because there is some variation in intensities on the tumor and since the algorithm uses grayscale intensity values it can't select different tissues densities without selecting a lot of healthy tissues. It can also be observed that even with the small thresholding such as the case in slice # 48, Figure 42(d), the algorithm selected a lot of pixels that are not part of the tumor.

The FP and FN rates of segmenting dataset #6 do not go lower than 80%. The images of the results of dataset 6 with a thresholding of 10% are shown in Figure 43. The algorithm is not capable of selecting the calcified pixels and soon the segmentation classifies healthy pixels as tumor pixels and grows to select the whole image as a tumor except for the calcified tumor, as shown in Figure 43(d). Resulting in a FP of 224% and a FN of 99%. Even if the algorithm selected most of the pixels it was incapable of selecting the actual tumor pixels when the tumor was calcified. The results of an increased thresholding of 20% only improve the FN by lowering it to 80% but a lot more pixels that are not part of the tumor are also selected and FP goes up to 283%.

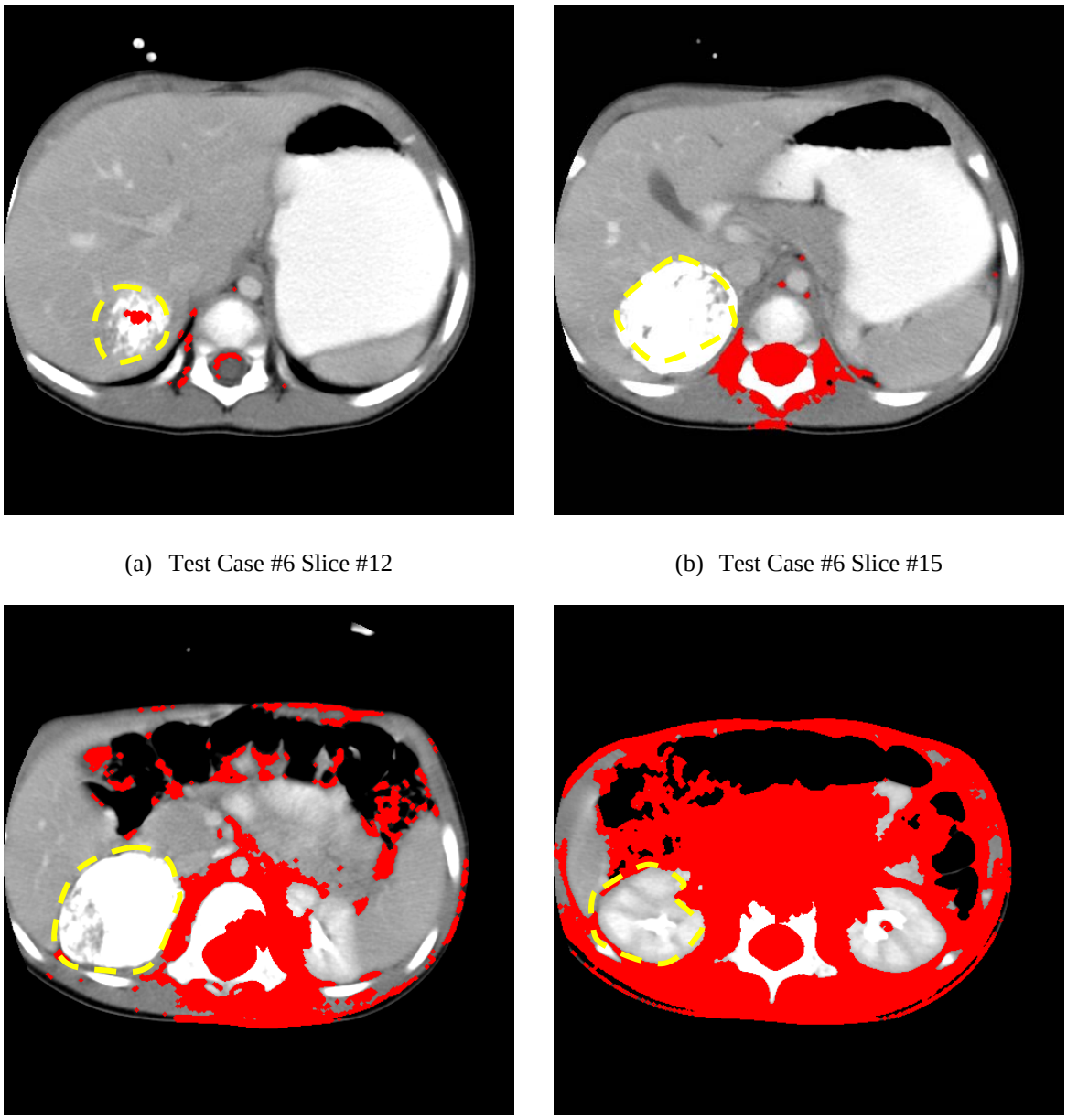

(a) Test Case #6 Slice #12

(b) Test Case #6 Slice #15

(c) Test Case #6 Slice #20

(d) Test Case #6 Slice #24

Figure 43. Grayscale Segmentation Results Case 6. Yellow outlines the approximate tumor, red is the actual segmentation by the algorithm**.**

Test Case #7 best results were a FP of 19% and a FN of 92%, these results can be observed in Figure 44. The FP rate is low because the algorithm does not select many of the pixels as shown in Figure 44(a), (b), and (c). The algorithm selects only one type of tissue

density and ignores the calcified tumor, or the pieces of tumor with different densities. As shown in Figure 44(c) the segmentation starts to grow and by the last slice Figure 44(d) the whole image is selected, except for the white pixels that in this case represent the actual tumor. The thresholding technique creates a region leak outside the tumor of densities similar in color with the region selected on the first slice but that unfortunately are not part of the actual calcified tumor.

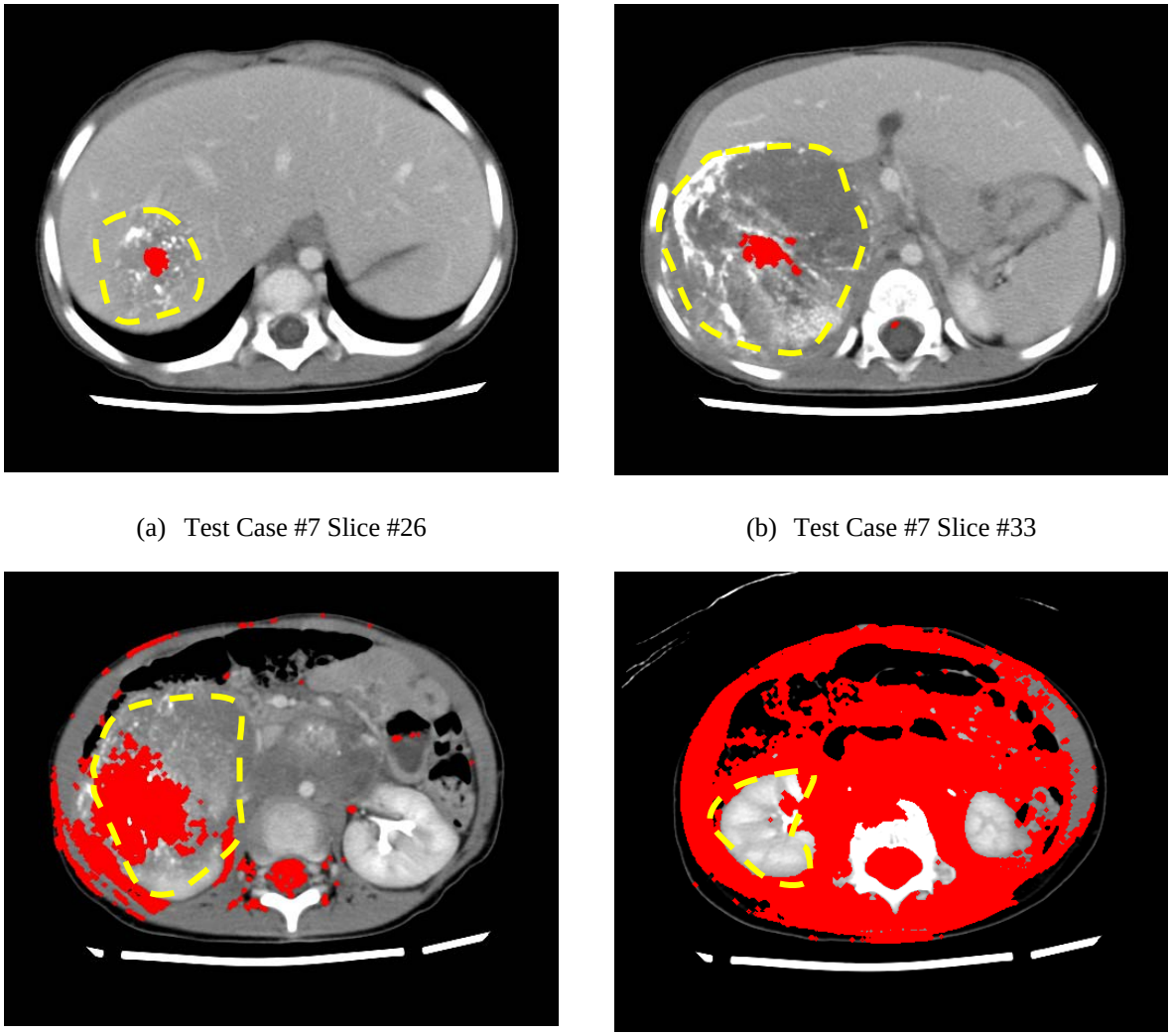

(a) Test Case #7 Slice #26

(b) Test Case #7 Slice #33

(c) Test Case #7 Slice #42

(d) Test Case #7 Slice #48

Figure 44. Test case #7. Yellow outlines the approximate tumor, red is the actual segmentation by the algorithm.

5.5.3 Limitations of Grayscale Thresholding

As the literature review of chapter 2 described and this section confirmed, basic thresholding does not yield acceptable segmentation results. If the tumor is density is very different than the healthy tissue density then this method produces adequate results as shown in test case #1, however if the tumor densities are similar to healthy tissues densities as in the case of test case #5, or if the tumor densities are varied as in test case #6 and test case #7 basic thresholding is not capable of producing results less than 90% in either FP or FN rates. In the following section the grayscale and color methods will be compared and it will be shown how adding color to the DICOM file and using the same thresholding technique but with information in the RGB channels yields much better results, even with category C tumors.

5.6 Comparison to other segmentation methods

While the results of the color segmentation are not as accurate as some other elaborate segmentation algorithms the segmentation algorithm implemented here was a basic thresholding technique that is not usually used for complex cases, comparing the segmentation of basic thresholding between the color and grayscale cases the color algorithms yielded much better results, as shown in Table 7 and Figure 45Figure 46. In each of the test cases the color algorithm yielded better results, especially in difficult cases. Test case #1 that corresponds to category A yielded the closest results between the two algorithms which is expected since in this case the tumor densities are very different to healthy densities and therefore simple thresholding can segment the tumor.

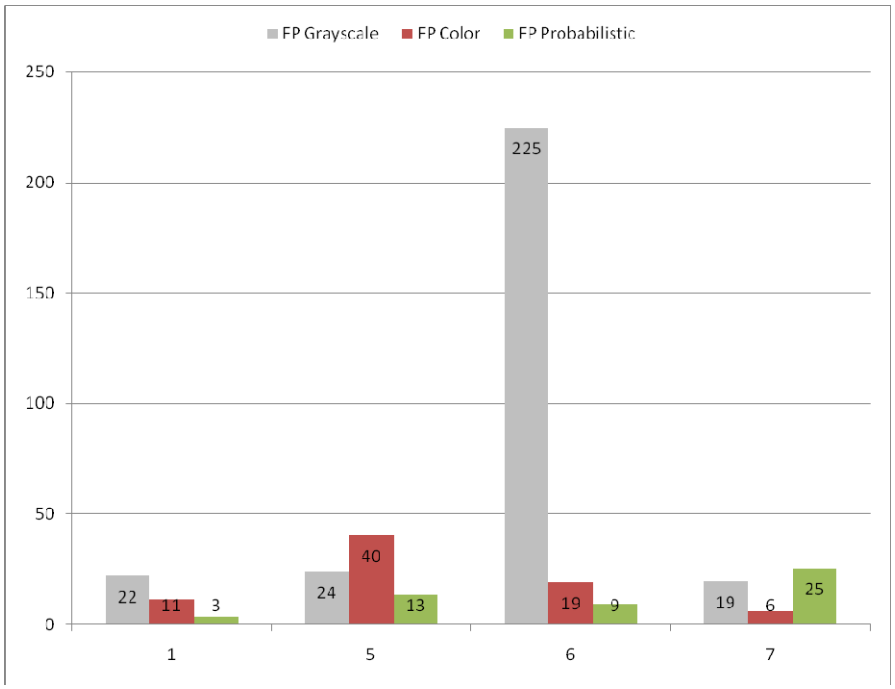

Figure 45. False Positive results for three segmentation methods: Grayscale (gray), Color (red), Probabilistic (green).

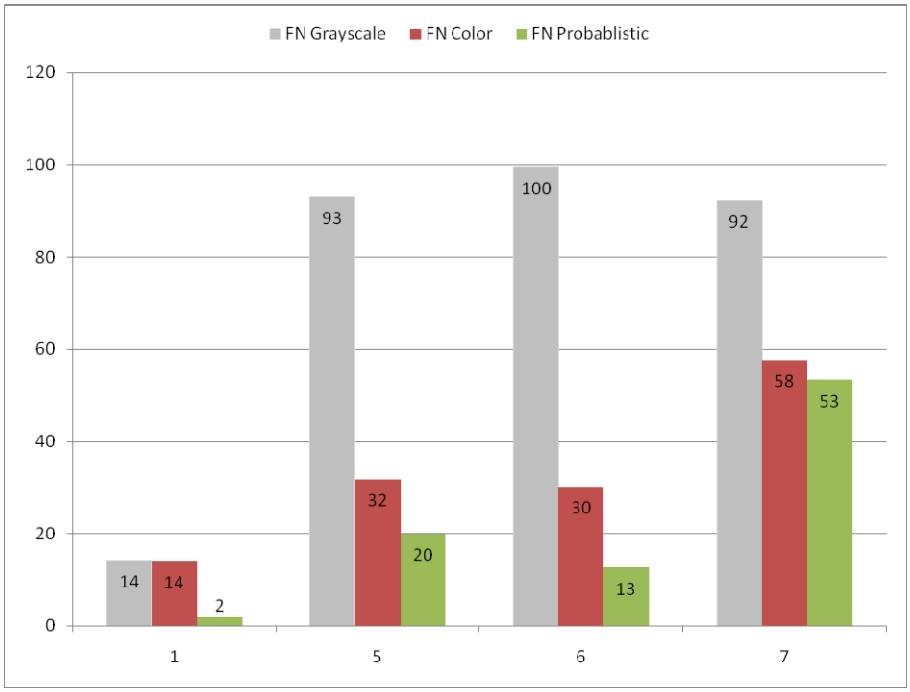

Figure 46. False Negative results for three segmentation methods: Grayscale (gray), Color (red), Probabilistic (green).

Table 7. Comparison between grayscale and segmentation with color pre-processing .

		Grayscale		Color		Probabilistic	
Test Case#	Category	FP	FN	FP	FN	FP	FN
1	A	21.8807	14.255	11.0837	14.0453	3.1000	1.8000
5	B	23.6672	93.077	40.3981	31.7252	13.1000	19.9000
6	B	224.641	99.545	18.8161	30.1461	9.1000	12.6000
7	C	19.2508	92.218	5.9099	57.6397	25.2000	53.4000

However calcified tumors or tumors with fuzzy edges or different tissue densities cannot be segmented accurately by grayscale thresholding methods as shown in test cases #5-#7 that had at least 90% FN, since most of the tumor pixels were not selected. Just by adding color to the image and performing the same thresholding algorithm in three channels the results improved as in case #6 from FP of 224% to 18% and false negative of 99% to 30%.

These results show that adding color to the DICOM file before performing segmentation improves the segmentation process.

A comparison between the color pre-processing and the probabilistic method [10] was also made and is shown in Figure 45Figure 46. The probabilistic method yielded better FN and FP results. All of the 10 cases yielded mean FN value of less than or equal to 25%. And eight out of the 10 cases yielded a mean FP value of less than or equal 25%. The color pre-processing method only yielded FP and FN values of less than 25% for half of the test runs. For test case #7 the color pre-processing method has around 6% of FP and 58% FN and the probabilistic method has a higher FN of 25% and a slightly lower FN of 53%. It is very important to highlight that the probabilistic method is a more complex method compared to the color thresholding technique used to test the color pre-processing.

As expected, the grayscale case produced the worst results, the probabilistic method yielded the best results and the color pre-processing method was in the middle. Even though the color pre-processing method did not yield the best results the results improved substantially the accuracy of the thresholding segmentation method. If the same approach is used for the probabilistic method, if color is added as a pre-processing step it could improve the accuracy of the current probabilistic method.

5.7 Timing

The method developed takes advantage of OpenGL textures to allow for the visualization of the segmentation results of the current slice in real time. For the twenty cases segmented the total time for the complete segmentation of the whole set was measured and then it was divided by the number of slices, the results are shown in Table 8. If segmentation is performed in the whole set of slices it takes a few seconds up to one minute if 251 slices are being segmented such as test case #6. Tweaking values on one slice is performed in real time, if the preferences selected to that slice want to be applied to the whole set then it takes an average of 1/10 of a second per slice to show the results.

Table 8. Segmentation Times per Test Case.

Dataset	Number of Slices	Threshold	Total Time	Time Slice
1	19	0.06	2.61	0.137368
1	19	0.05	2.63	0.138421
2	90	0.38	15.38	0.170889
2	90	0.45	15.2	0.168889
3	251	0.25	50.1	0.199602
3	251	0.1	61.19	0.243785
4	4	0.25	0.43	0.1075
4	4	0.2	0.43	0.1075
5	31	0.11	5.08	0.163871
5	31	0.2	5.4	0.174194
6	13	0.45	1.42	0.109231
6	13	0.47	1.53	0.117692
7	23	0.1	2.99	0.13
7	23	0.1	2.9	0.126087
8	16	0.4	2.02	0.12625
8	16	0.3	2	0.125
9	17	0.3	1.83	0.107647
9	17	0.15	1.64	0.0964706
10	12	0.36	1.4	0.116667
10	12	0.28	1.38	0.115
			Average per slice	0.1391032

5.8 Limitations of the segmentation algorithm using color pre-processing

While the algorithm shows promising results especially in comparison of grayscale thresholding, there are several limitations to the current method. One of them is the importance of the user input, the user needs to select a region of interest, then place a seed, and in most cases tweak with minimum and maximum colors to get the best segmentation results. If the user does not know about the tumor, or selects the wrong initial region or places the seed in the correct place the algorithm does not select the appropriate pixels. While it is true that in the easy cases the algorithm is capable of detecting the tumor with low FP

and FN rates without the need of tweaking with the minimum and maximum colors, the user still has to select a region of interest and place a seed.

Since this method is thresholding on three different channels the method is very sensitive to tissue densities. In some cases if the color values are varied even by a little bit the results vary a lot. For example test case #4, using the same threshold of 25% if the color minimum is moved from 109 to 112, 3 values and the color maximum is decreases from 55 to 41, 14 values, the FP changes from 54% to 76% and FN changes from 33% to 11%. Because the algorithm is only dependant on the position and on the densities if the wrong maximum color and minimum color are chosen then the resulting FN and FP ranges will be very high.

Due to the fact of the high sensitivity of the tissue densities the method also performs poorly when the densities within a tumor are varied, selecting only a few pixels of the tumor such as in test case #6 and #7, however it does not select a lot of pixels outside the tumor. In a similar fashion when the edges of the tumor are fuzzy such as in cases #9-#10 the algorithm picks a lot of pixels that are not part of the tumor.

6. CONCLUSIONS

6.1 Summary of conclusions

A framework to improve the accuracy of tumor segmentation from medical image data was presented. This framework includes an interface for visualization of DICOM data in 2D and 3D. The framework introduced the idea of colorizing medical image by selecting a region of interest, usually the tumor and colorizing the rest of the image with RGB values in a linear fashion. This method also takes advantage of OpenGL textures to allow interactive segmentation by having user tweak with the parameters in real time and visualize the results.

In the past colorization techniques have been implemented to achieve better visualization results, such as colorizing black and white movies, however colorization methods in medical image data to improve segmentation is a novel concept. To prove the concept that colorizing or adding R, G, and B channels, information to an image to improve segmentation a basic thresholding technique was implemented in grayscale and in color. The method was very similar; the only difference was that instead of calculating the difference between the original HU values for the grayscale case, the difference was calculated in RGB, in three channels. The new method performed a lot better than the grayscale method in all the cases, but especially in difficult cases tumors with calcification or tumors with different densities. While the grayscale method had FN values of 90%, the color case had FN values up to 57%. 10 out of the 20 test cases gave false positives of 25% or less, and 10 out of the 20 test runs gave false negatives of 25% or less. This new method promises a lot of possibilities, however future work has to be done on the proposed method.

It is important to note that at this point human input is fundamental to this method and segmentation methods in general. The segmentation algorithms developed to this day are not completely accurate and when the results are helping to determine surgical planning there is no room for errors.

6.2 Future work

Future work on this framework can be divided into four ways: (a) adding different and more complex segmentation algorithms using color information; (b) trying different color pre-processing methods (c) using GPU and shaders to increase the speed of the results; (d) different ways to move the seed point; (e) isolate the sources of error; (g) improve the user interface.

Taking into account that adding color to the basic grayscale thresholding technique improved results there is a possibility that adding more complex color segmentation algorithms can yield even better results. Many successful algorithms that are used for tumor segmentation are only focused on grayscale methods since medical data is obtained only in reference to HU values. If adding color to the images improves the basic method other methods can also be improved in this fashion. Probabilistic segmentation methods, fuzzy logic, and region grow can be methods to be tested using color pre-processing techniques and then segmentation. These new methods may decrease the need of user input.

A simple color pre-processing method that added RGB information from red to blue in a linear fashion was implemented, however other methods can also be tested to see if they improved segmentation results. Adding more colors instead of just RGB or even changing

color spaces for example using HSI instead of RGB may yield different results that could make the framework more robust.

The method proposed in this work uses textures to visualize the results to be tweaked in real time. Using shaders offers another possibility instead of generating textures every time a parameter is changed, and perhaps shaders will improve the speed of the method. While the method is already fast improving the speed allows for more complicated methods to be implemented without sacrificing the speed of the framework.

The method only explores one way to move the seed point which is by placing the seed on the center of the previous segmented slice. Other ways to move the seed point may yield better results and should be explored in future work.

Several parameters are used to calculate the segmentation region and it is not clear which parameters have the most influence on the results, a study needs to be developed to isolate the sources of error in the method and segmentation in general.

The user interface right now has not been tested and has only been used by the developers. Testing should be performed to improve the user experience and make the application easier to use.

ACKNOWLEDGMENTS

I would first like to acknowledge my parents and my brother. Also my extended family which includes my grandparents, uncles, cousins and my old friends: “the band”, the “pecados”, and the fantastic four. You always believed in me and helped me to get into a better university even if it meant being away from all of you, and you motivated me to take advantage of the great opportunity.

I also want to thank Eliot Winer because he gave me the opportunity to do a masters. He was patient with my lack of programming skills and at the same time pushed me enough to try new things and learn more.

To Eric Foo because he was there day through day helping me with concepts, code, and the revision of this thesis.

Ken Kopecky because when I asked if I should do A or B he said C, which was very complicated at first but resulted in a big important part of my research. Also because when I see his code I think pretty and it pushes me to improve my coding skills.

To the watch research group especially Vijay K, Brandon N, Catherine P, Andrew k because they helped me with random stuff from makefile files to Socketing.

And to all my friends, especially Curt Putney, Grego Worhland, Jason Morgan, Len Martinez, Al Cosme, and Nick Johnston because they have helped a lot in the last few months with things like posters, to grammar and spelling.

REFERENCES

[1] Gonzalez, Rafael C., and Richard E. Woods. Digital Image Processing. New York: Addison-Wesley, 2008.

[2] Bankman, Isaac. Handbook of Medical Imaging: Processing and Analysis. California: Academic Press, 2000.

[3] Imaginis: Brief History of CT. 13 Sep. 2007. Imaginis. 22 Oct. 2008. <http://www.imaginis.com/ct-scan/history.asp>

[4] Hornak, Joseph. The Basics of MRI. 22 Oct. 2008. <http://www.cis.rit.edu/htbooks/mri/inside.htm>

[5] Nema. Digital Imaging and Communications in Medicine. 22 Oct. 2008 <http://medical.nema.org/>

[6] Pham, Dzung.L., Chenyang Y. Xu, and Jerry L. Prince. "A Survey of Current Methods in Medical Image Segmentation." Medical Image Analysis 2.1 (1998): 1-36.

[7] Ayres, F.J, et al. "Estimation of the Tissue Composition of the Tumor Mass in Neuroblastoma Using Segmented CT Images." Medical & Biological Engineering and Computing 42.3 (2004): 266-77.

[8] Intuitive Surgical: da Vinci Surgical System. 22 Oct. 2009. <http://www.intuitivesurgical.com/products/davinci_surgicalsystem/index.aspx>

[9] Marescaux, Jaques., et al. "Transcontinental Robot-Assisted Remote Telesurgery: Feasibility and Potential Applications." Annals of Surgery 245.4 (2002): 487-92.

[10] Foo, Eric. “A Framework for Segmentation and Interactive Immersive Visualization of Medical Image Data.” Diss. Iowa State University, 2008.

[11] Pham, Dzung L., Chenyang Xu, and Jerry L. Prince. “Current Methods in Medical Image Segmentation.” Annual Review of Biomedical Engineering 2 (2000): 315-337.

[12] Clarke, L.P. et al. “MRI Segmentation: Methods and Applications.” Magnetic Resonance Imaging 13.3 (1995): 343-68.

[13] Hadwiger, Marcus, et al. State of the Art Report 2004 on GPU Based Segmentation. Vienna, Austria: VRVis Research Center, 2004.

[14] Fan, Jianping, et al. “Automatic Image Segmentation by Integrating Color-Edge Extraction and Seeded Region Growing.” IEEE Transactions on Image Processing 10 (2001): 1454-66.

[15] Rajapakse, Jagath C., et al. “Statistical Approach Segmentation Single-Channel Cerebral MR Images.” IEEE Transactions on Medical Imaging 16 (1997): 176-86.

[16] Sezgin, Methmet, and Bulent Sankur. “Survey Over Image Thresholding Techniques and Quantitative Performance Evaluation.” Jounral of Electronic Imaging 13.1 (2004): 146-65.

[17] Freixenet, F., et al. “Yet Another Survey on Image Segmentation: Region and Boundary Information Integration.” Lecture Notes In Computer Science: Proceedings of the 7th European Conference on Computer Vision-Part III, Denmark, 28-31 May 2002. Ed. A Hayden. Berlin: Springer, 2002. 408-422.

[18] Hojjatoleslami, S.A., and J. Kittler. “Region Growing: A New Approach.” IEEE Transactions on Image Processing 7 (1998): 1079-84.

[19] Pohle, Regina, and Klaus, Toennies. “Segmentation of Medical Images Using Adaptive Region Growing.” SPIE Medical Imaging 4322 (2001): 1337-46.

[20] Berkhin, P. “Survey in Clustering Data Mining Techniques.” Grouping Multidimensional Data: Recent Advances in Clustering. Ed. Jacob Kogan. Berlin: Springer, 2006. 25-71.

[21] Zhang, Dao-Qiang, and Song-Can Chen. “A Novel Kernelized Fuzzy C-means Algorithm with Application in Medical Image Segmentation.” Artificial Intelligence in Medicine 32.1 (2004): 37-50.

[22] Held, Karsten, et al. “Markov Random Field Segmentation of Brain MRI Images.” IEEE Transactions on Medical Imaging 16 (1997): 878-886.

[23] Zhang, Yongye, et al. “Segmentation of Brain MR Images through a Hidden Markov Random Field Model and the Expectation-maximization Algorithm.” IEEE Transactions on Medical Imaging 20 (2001): 45-57.

[24] Vincken, Koen. “Probabilistic Multiscale Image Segmentation. “ IEEE Transactions on Pattern Analysis and Machine Intelligence 19 (1997): 109-120.

[25] Xu, Chenyang, et al. “Image Segmentation Using Deformable Models.” Handbook of Medical Imaging: Medical Image Processing and Analysis. Ed. Jacob Beutel. Bellingham: SPIE Press, 2000. 129-74.

[26] Kaus, Michael R., et al. “Automated Segmentation of the Left Ventricle in Cardiac MRI.” Medical Image Analysis 8.3 (2003): 245-54.

[27] McInerney, Tim, and Demetri Terzopoulos. “Deformable Models in Medical Image Analysis: a Survey.” Medical Image Analysis 1.2 (1996): 91-108.

[28] Reddick, Wilburn E., et al. “Automated Segmentation and Classification of Multispectral Magnetic Resonance Images of Brain Using Artificial Neural Networks.” IEE Transactions on Medical Imaging 16 (1997): 911-18.

[29] Huang, Yu-Len, and Dar-Ren Chen. “Watershed Segmentation for Breast Tumor in 2-D Sonography.” Ultrasound in Medicine & Biology 30.5 (2004): 625-32.

[30] Egmont-Patersen, M., D. de Ridder, and H. Handels. “Image Processing with Neural Networks – a Review.” Pattern Recognition 35 (2002): 2279-301.

[31] Saha, Punam K, Jayaram K . Udupa, and Dewey Odhner. “Scale-Based Fuzzy Connected Image Segmentation: Theory, Algorithms, and Validation.” Computer Vision and Image Understanding 77 (2000): 145-174.

[32] Udupa, Jayram K., and Supun Samarasekera. “Fuzzy Connectedness and Object Definition: Theory, Algorithms, and Applications in Image Segmentation.” Graphical Models and Image Processing 58 (1996): 246-61.

[33] Moonis, Gul, et al. “Estimation of Tumor Volume with Fuzzy-Connectedness Segmentation of MR Images.” American Journal of Neuroradiology 23 (2002): 356-63.

[34] Lorenzo-Valdés, M., et al. “Atlas-Based Segmentation and Tracking of 3D Cardiac MR Images Using Non-rigid Registration.” Medical Image Computing and Computer-Assisted Intervention-MICCAI 2002, 5th International Conference Proceedings, Tokyo, 25-28 September 2002. Ed. Takeyoshi Dohi. Berlin: Springer. 642-50.

[35] Gibou, Frédéric, and Ronald Fedkiw. A Fast Hybrid k-Means Level Set Algorithm for Segmentation. California: Standford University Computer Science Department, 2002.

[36] Atkins, M. Stella, and Blair T. Mackiewich. “Fully Automatic Segmentation of the Brain in MRI.” IEEE Transactions on Medical Imaging 17 (1998): 98-107.

[37] Cheng, H.D., et al. “Color Image Segmentation: Advances and Prospects.” Pattern Recognition 34 (2001): 2259-81.

[38] Levin, Anat, Dani Lischinski, and Yair Weiss. “Colorization Using Optimization.” Proceedings of the 2004 SIGGRAPH Conference. Ed. John C.Hart. New York: ACM, 2004. 689-94.

[39] Welsh, Tomihisa, Michael Ashikhim, and Klaus Mueller. “Transferring Color to Greyscale Images.” International Conference on Computer Graphics and Interactive Techniques: Proceedings of the 29th Annual Conference on Computer Graphics and Interactive Techniques, San Antonio, Texas, 23-26 July 2002. New York: ACM, 2002. 277-80.

[40] Sapiro, Guillermo. “Inpainting the Colors.” IEEE International Conference on Image Processing, 2005. 2005. 698-701.

[41] Pfister, Hanspeter, et al. “The Transfer Function Bake-off.” IEEE Computer Graphics and Applications 21 (2001): 16-22.

[42] He, Taosong, et al. “Generation of Transfer Functions with Stochastic Search Techniques.” IEEE Visualization: Proceedings of the 7th Conference on Visualization ’96, San Francisco, California, 28-29 October 1996. Ed. Roni Yagel. CA: IEEE Computer Society, 1996. 227-34.

[43] Yatziv, Liron, and Guillermo Sapiro. “Fast Image and Video Colorization Using Chrominance Blending.” IEEE Transactions on Image Processing 15 (2006): 1120-29.

[44] Blasi, Di, and Reforgiatio Recupero. “Fast Colorization of Gray Images.” Proceedings Eurographics Italian Chapter, 2003. 2003.

[45] Chen, Tongbo, et al. “Grayscale Image Matting and Colorization.” Proceedings of Asian Conference on Computer Vision, Korea, 2004. 2004. 1165-69.

[46] Horiuchi, Takahiko, and Sayaka Hirano. “Colorization Algorithm for Grayscale Image by Propagating Seed Pixels.” International Conference on Image Processing, 2003. 2003. 457-60.

[47] Tzeng, Fan-Yin, Eric B. Lum, and Kwan-Liu Ma. “A Novel Interface for Higher-Dimensional Classification of Volume Data.” Proceedings of the 14th IEEE Visualization, 22-24 October 2003. Washington, DC: IEEE Computer Society, 2003. 505-12.

[48] Silverstein, Jonathan C., Nigel M. Parsad, and Victor Tsirline. “Automatic Perceptual Color Map Generation for Realistic Volume Visualization.” Journal of Biomedical Informatics 41 (2008): 927-35.

[49]Pelizzari, Charles A., et al. “Volumetric Visualization of Anatomy for Treatment Planning.” International Journal of Radiation Oncology, Biology and Physics 34.1 (1996): 205-11.

[50] Li, C.H., and P.C. Yuen. “Regularized Color Clustering in Medical Image Database.” IEEE Transactions on Medical Imaging 19 (2000): 1150-55.

[51]Lucchese, L., and S.K. Mitra. “Color Image Segmentation: A State-of-the-Art Survey.” Proceedings Indian National Science Academy, India. 2001. 207-21.

[52] Skarbek, Wladyslaw, and Andreas Koschan. “Colour Image Segmentation – A Survey - .” Berlin: Institute for Technical Informatics, University of Berlin, 1994.

[53] Lin, Xueyin, and Shaoyun Chen. “Color Image Segmentation Using Modified HSI System for Road Following.” IEEE International Conference on Robotics and Automation, Proceedings, California, 9-11 April 1991. 1991. 1996-2003.

[54] Cheng, H.D., X.H. Jiang, and Jingli Wang. “Color Image Segmentation Based on Homogram Thresholding and Region Merging.” Pattern Recognition 35 (2002): 373-93.

[55] Verikas, A., K. Malmqvist, and L. Bergman. “Colour Image Segmentation by Modular Neural Network.” Pattern Recognition Letters 18 (1997): 173-85.

[56] Cremers, Daniel, Mikael Rousson, and Rachid Deriche. “A Review of Statistical Approaches to Level Set Segmentation: Integrating Color, Texture, Motion and Shape.” International Journal of Computer Vision. 72 (2006): 195-215.

[57] Volview. 8 Nov. 2008 <http://www.kitware.com/products/volview.html>

[58] OsiriX Imaging Software. 9 Nov. 2008 < http://www.osirix-viewer.com/>

[59] “Morphology Fundamentals: Dilation and Erosion.” The MathWorks. 9 Nov. 2008 <http://www.mathworks.com/access/helpdesk/help/toolbox/images/index.html?/access/helpdesk/help/toolbox/images/f18-12508.html>

[60] DCMTK – DICOM Toolkit. 9 Nov. 2008 <http://dicom.offis.de/dcmtk>

[61] OpenGL. 9 Nov. 2008 <http://www.opengl.org/>

[62] The Visualization Toolkit (VTK). 9 Nov. 2008 <http://www.vtk.org/>

[63] Corona. 9 Nov. 2008 <http://corona.sourceforge.net/>

[64] VR Juggler. 9 Nov. 2008 <http://www.vrjuggler.org/>